DROPLET PENETRATION METHOD AS A WETTABILITY TEST FOR PHARMACEUTICAL POWDERS

By

YU HAN

A thesis submitted to the
Graduate School – New Brunswick
Rutgers, The State University of New Jersey
In partial fulfillment of the requirement
For the degree of
Master of Science
Graduate Program in Chemical and Biochemical Engineering
Written under the direction of
Dr. German Drazer and Dr. Gerardo Callegari
And approved by

_____

_____

_____

New Brunswick, New Jersey
May, 2017

ABSTRACT OF THE THESIS

Droplet Penetration Method as a Wettability Test for Pharmaceutical Powders

By YU HAN

Thesis Director:

Dr. German Drazer and Dr. Gerardo Callegari

A droplet penetration method (DPM) was developed to characterize the wettability of pharmaceutical powders. Sessile droplets of two different liquids, used as *test* and *reference* liquids, were deposited on a slightly compressed powder bed and their penetration processes was recorded. Two simplifying assumptions are considered. First, the capillary pressure inside the porous powder is the only dominant driving force for the imbibition of drops. Second, the contact area between the penetrating drop and the powder bed is constant. Then, the penetration process in non-dimensional variables is independent of any dimensionless number. Hence, a *reference* liquid can be used to decouple the properties of the powder bed from the assessment of contact angle of the *test* liquid.

In this thesis, the effect of particle size distribution on the wetting behavior of pharmaceutical powders was investigated by the droplet penetration method. Two powder materials, an excipient and an active pharmaceutical ingredient (API), are used. The excipient is lactose monohydrate powder sieved to obtain particles in the following size

ranges: 38-45, 45-53, 53-63, 63-75, 75-90, 90-106 μm. The API used is caffeine anhydrous powder with particle size distribution characterized by d50 = 15, 19 and 30 μm. In all cases, the test liquid is deionized water and the reference liquid used was silicone oil. It was found that lactose powders with a particle size smaller than 75 μm have approximately the same contact angle. However, there is a significant decrease in the calculated contact angle when particles are larger than 75 μm. In the case of caffeine, it was found that larger particles yield smaller contact angle.

Acknowledgement

I would first like to thank my thesis advisors, Dr. German Drazer and Dr. Gerardo Callegari, for giving me the opportunity to work on this project and encourage me to devote my thesis on it. Their inspiring advices, patient instructions and immense support guided me throughout my research.

I would also like to thank the Engineering Research Center for Structured Organic Particulate Systems (ERC-SOPS) for providing all the resources and facilities needed in my research. I would like to express my sincere appreciation to Zhanjie Liu, who has been with me throughout my research on droplet penetration project, his insightful guidance and assistances are essential in this project. I would like to thank Dr. Sara Moghtadernejad whose precious suggestion and discussion always guided me toward a more professional way. My sincere thankfulness is also given to Vineeth Krishnamsetty and Muhammad Sharif who have provided great assistance to my experimental works.

Table of Contents

Chapter 1. Introduction

Wettability of pharmaceutical powder

Powders to be manufactured into solid dosage form, like tablet, are ubiquitous in the pharmaceutical industry. The important role of characterizing their wettability has long been recognized. (Lerk, 1976) (Buckton, 1993) Knowing the wetting properties of both excipients and the active pharmaceutical ingredient is crucial to a number of processes, ranging from formulation development to the manufacturing process. For example, wetting of tablets inside the digestive system can affect the rate of their disintegration, dispersion and dissolution. Therefore, it is critical to consider the wettability as one of the important properties in designing formulation and controlling drug delivery. (Holm, 2016)

Another example of reasons for studying wettability of powder in pharmaceutical research and development is the wet granulation. It is a process to bind powders together to form larger multiparticle granules by using a binding agent. In the granulator, liquid bridges will be formed between primary powders before solvent dries. The wetting properties of powders can affect the performance of granulation solution, and hence are in demand for selecting the solvent of binding solution. (Zhang, 2002) In addition, the wetting properties of excipient powders, in some cases, are correlated with other critical quality attributes of solid dosage forms, such as tablet hardness. (Pawar, 2016) (Razavi, 2016)

As a result, many experimental methods to measure the contact angle of pharmaceutical powders are developed. In this thesis, we focus on the droplet penetration method (DPM),

in which the wettability of a powder is characterized by the penetration dynamic of a sessile drop deposited on a slightly compressed powder bed. (Liu, 2017)

Droplet penetration method

The idea of DPM has been used widely in a number of areas, besides pharmaceutical industry, to characterize the wetting properties of powders, granular materials, and porous media. For example, in soil sciences, the water-drop penetration time (WDPT) test is a traditional method to characterize soil hydrophobicity or water repellency. (Buczko, 2006) Another application of this idea relates to spreading and penetration of surfactant-laden drops on thin-permeable media (like papers) with reference to ink-jet printing or functionalization of textile fabric. (Daniel, 2006) (Gambaryan-Roisman, 2014)

DPM has some comparative advantages over other methods, also based on the dynamic of liquid penetration into the powder, like Washburn capillary rise. For example, it has a relatively simpler set-up design. It usually takes a shorter time for slightly compressed powder bed. And it consumes less liquid to perform experiments compared with capillary rise method. We don't discuss more details of benefits and disadvantages of DPM over other wettability tests in this thesis. Here is a recommended reference with detailed discussion about DPM and alternative characterization methods. (Alghunaim, 2016)

Effect of Particle Size Distribution on Wettability of Powder

T. Dang-Vu et al. have concluded that particle size does not have significant effect, which can be observed by capillary rise method, on contact angle of porous bed. (Dang-Vu, 2005) Similarly, Stevens, N. et al. reported no importance of particle size within

range of 40-200um on contact angle by using glass spheres and crushed quartz. (Stevens, 2009) However, Kirchberg et al. has showed the effect of particle size distribution of magnetic micropowders on their wettability by Washburn capillary test. Larger particle sizes yield smaller contact angle between water and magnetic powders. (Kirchberg, 2011)

Note that using different powder materials can yield different conclusions on the influence of particle size on contact angle. In this thesis, we are interested in studying the pharmaceutical powders, which include both excipients and active pharmaceutical ingredients. If the particle size influence significantly on the wetting behaviors of powders, measurements of contact angle with variation of particle size should be critical to find the desired particle size for both manufacturing process and drug delivery. The excipient we tested is lactose monohydrate powder and the API is anhydrous caffeine powder.

Powder Materials

- **Lactose Monohydrate ($C_{12}H_{24}O_{12}$)**

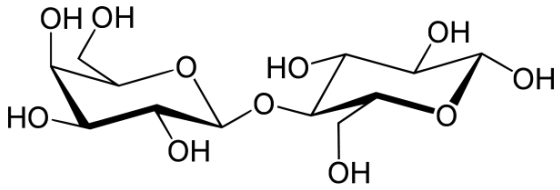

(From: https://en.wikipedia.org/wiki/Lactose)

Lactose ($C_{12}H_{22}O_{11}$) is a disaccharide sugar composed

of galactose and glucose that is found in milk. The molecular structure shown above is β-D-galactopyranosyl-(1→4)-D-glucose, which is a IUPAC name.

Lactose is widely used as a filler or filler-binder in the manufacture of pharmaceutical tablets and capsules. The general properties of lactose that contribute to its popularity as an excipient are its cost effectiveness; availability; bland taste; low hygroscopicity; compatibility with active ingredients and other excipients; excellent physical and chemical stability and water solubility. (Guo, 2004)

The most common form of lactose used in pharmaceutical formulation is crystalline α-lactose monohydrate. This form is available in a range of milled and sifted pharmaceutical grades differing in physical properties, such as flowability, bulk density, and particle size distribution.

- **Anhydrous caffeine**

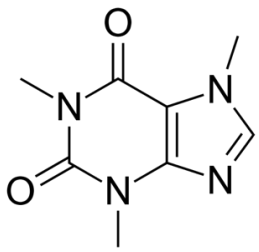

(From: https://en.wikipedia.org/wiki/Caffeine)

Caffeine is a bitter, white crystalline purine, a methylxanthine alkaloid, and is chemically related to the adenine and guanine bases of deoxyribonucleic acid (DNA) and ribonucleic acid (RNA). It is found in the seeds, nuts, or leaves of a number of plants native to South America and East Asia and helps to protect them against predator insects and prevent germination of nearby seeds. The most well known source of caffeine is the coffee bean, a misnomer for the seed of Coffea plants.

Caffeine is a central nervous system (CNS) stimulant of the methylxanthine class. (Nehlig, 1992) It is the world's most widely consumed psychoactive drug. Unlike many other psychoactive substances, it is legal and unregulated in nearly all parts of the world.

It can treat and prevent the premature infant breathing

disorders bronchopulmonary dysplasia of prematurity and apnea of prematurity.

Chapter 2. Theory

2.1 Governing equations

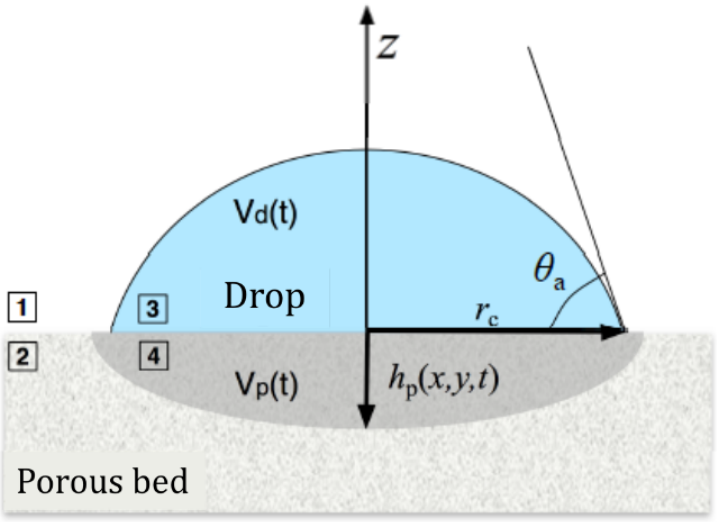

Fig 1 Schematic view of a sessile drop penetrating into a porous powder bed: (1) Air; (2) Porous bed; (3) Sessile drop, drop volume above the bed surface $V_d(t)$; (4) Wet region inside of the powder bed. The position of the interface between the wet and dry regions inside of the powder bed is given by $z = -h_p(x, y, t)$. (Liu, 2017)

The governing equations describe the penetration process of a sessile drop deposited on the surface of a powder bed. The scheme is shown in Fig. (1). We consider that the penetration on powder bed has some significant similarities with experiments on the capillary rise of a fluid into a porous medium. At short times, particularly, fluid inertia dominates the dynamic (Ridgway, 2002) (Quéré, 1997) (Bosanquet, 1923), and we ignore these effects limiting our theory to a larger time scales. For the fully developed scale after short times, we shall assume that the transport of fluid inside of the powder bed follows Darcy's law:

$$\mathbf{u} = -\frac{k}{\mu}\nabla p \tag{1}$$

where $\mathbf{u} = (u_x, u_y, u_z)$ is the volume-averaged fluid velocity, also called *superficial* velocity or *specific discharge*, μ is the dynamic viscosity of fluid, and k is the permeability of the powder bed. Darcy's law suggested a macroscopic description of transport inside of the powder bed (Dullien, 2012) (Bear, 2013). Also, we assume that the inside of powder bed is homogeneous and isotropic at the macroscopic level, which leads to a uniform scalar permeability of the bed.

Neglecting the liquid evaporation inside of the porous bed and assuming incompressibility of liquid, continuity equation for $\mathbf{u}$ can be written:

$$\nabla \cdot \mathbf{u} = 0 \tag{2}$$

Combination of Eqn. (1) and Eqn. (2) will yield the Laplace equation for the pressure field

$$\nabla^2 p = 0 \tag{3}$$

In principle, we should also consider the governing equation describing the evolution of the fluid inside of the drop over the powder bed surface. However, we shall see it is trivial to do so. We shall approximate the pressure inside of the drop to be uniform and equal to the atmospheric pressure, p_0, at all time. (Liu, 2017) First, we assume the pressure drop that develops due to the fluid motion inside of the drop is small compared to the pressure differences that move the fluid through microscopic pore space inside of the porous bed. We also assume that the size of the drop is much larger than the pore size, for example, 1 mm compared with 1 um. Thus, the pressure difference across the drop-air interface over the bed surface is negligible compared to the capillary pressure at the liquid-air interface inside of the porous bed. In addition, we neglect gravity effects on the

pressure of liquid both inside the drop and bed. Therefore, it is not necessary to assume that the drop size is below the capillary length. In other words, the analysis could still apply for a drop that deforms under gravity (Liu, 2017), which allows a larger size range of drop deposited on the bed.

2.2 Boundary Conditions

We define the penetration profile or *wetting front*, $h_p(x, y, t)$ by an implicit equation, following the notation used in Ref. (Alleborn, 2004)

$$F(x, y, z, t) = h_p(x, y, t) + z = 0 \tag{4}$$

The kinematic condition then couples the evolution of the wetting front to the flow field inside of the powder bed

$$\frac{DF}{Dt} = \frac{\partial F}{\partial t} + (\mathbf{v} \cdot \nabla)F = \frac{\partial h_p}{\partial t} + v_x \frac{\partial h_p}{\partial x} + v_y \frac{\partial h_p}{\partial y} + v_z = 0 \tag{5}$$

where $\mathbf{v}$ is the *interstitial* or *seepage* velocity, $\mathbf{u} = \varepsilon \mathbf{v}$, where ε is the porosity of the medium. The description of the penetration profile should be consistent with the description of the flow, thus, performed at the same macroscopic level as Darcy's law. As a result, the kinematic condition does not account for the complex pore space of the powder bed. Similarly, the dynamic boundary condition inside the medium is the normal-stress balance

$$p|_{F\,=\,0} - p_0 = -p_c \tag{6}$$

where we assume that the pressure inside of the dry powder is equal to the atmospheric pressure, p_0, and p_c is the capillary pressure (we use the convention that p_c is positive when the liquid wets the powder) (Bear, 2013). Note that any pressure build-up due to the displacement of air by the penetrating liquid is negligible compared with the corresponding pressure drop driving the liquid penetration.

Based on the macroscopic nature of the equation above, it is necessary to write the capillary pressure explicitly in terms of the wetting properties of the powder and the packed structure of the powder bed. To be specific, we could write an effective Young-Laplace equation for the normal-stress condition, which is our first boundary condition

$$p|_{F=0} - p_0 = -p_c = -\frac{2\gamma\cos\theta}{r_{eff}} \tag{7}$$

where γ is the surface tension, θ is the contact angle of the liquid on the powder, and r_{eff} is the *effective pore radius*, that is, the radius of a capillary made of the powder material that would result in the same capillary pressure as that in the macroscopic description (Liu, 2017). We shall also assume the capillary pressure is independent of the position of the wetting front, as a result of homogeneous porous bed.

Finally, we consider the boundary condition at the inlet of the penetration, where is the interface between powder bed and the drop above it. We shall assume that the contact radius r_c (see Fig. (1)) is constant during the penetration, or at least, during a significant portion of the penetration process. The portion will be used to calculate the contact angle. In this case, the boundary conditions at the powder bed-sessile drop interface correspond to continuity conditions in both pressure and velocity fields. Recalling that the pressure inside of the sessile drop is approximated as equal to the atmospheric pressure, we have

$$p(x,y,z,t)|_{z=0} = p_0 \qquad \text{for } r \le r_c \tag{8}$$

2.3 Scaling and Nondimensionalization

Given the conditions and approximations discussed above, we can identify the appropriate characteristic scales for the drop penetration process. First of all, we have ignored the flow and pressure fields inside of the sessile drop. In addition, capillary

pressure resulting from the drop-air interface can also be neglected. As a result, the initial radius R_0 and initial volume $V_0 = V_d(t = 0)$ of the sessile drop have no effect on the penetration dynamic, except through the change of contact radius r_c. In fact, only the contact radius appears in the governing equations and boundary conditions, giving the area of penetration inlet region in Eqn. (8).

Therefore, we take the contact radius as the characteristic length $l_c = r_c$ (Liu, 2017).

$$l_c = r_c \tag{9}$$

The characteristic scale of pressure field inside of the powder bed is given by the Eqn. (7). Hence the characteristic velocity u_c can subsequently be obtained from Darcy's law Eqn. (1)

$$u_c = \frac{kp_c}{\mu r_c} \tag{10}$$

Finally, we define the characteristic time for the convective transport inside of the bed

$$t_c = \frac{r_c}{v_c} = \frac{\varepsilon r_c}{u_c} = \frac{\mu \varepsilon {r_c}^2}{kp_c} \tag{11}$$

Next, we can use the identified characteristic velocity, time, length and pressure scales to obtain the nondimentional governing equations. (Liu, 2017)

$$\overline{\mathbf{u}} = -\overline{\nabla}\,\overline{p} \tag{12}$$

$$\overline{\nabla}^2\,\overline{p} = 0 \tag{13}$$

where $\overline{x} = x/r_c, \overline{y} = y/r_c, \overline{z} = z/r_c$ and $\overline{p} = p/p_c$.

Similarly, we obtain the nondimensional boundary condition for the liquid front

$$\frac{\partial \overline{h_p}}{\partial \overline{t}} + \overline{u_x}\frac{\partial \overline{h_p}}{\partial \overline{x}} + \overline{u_y}\frac{\partial \overline{h_p}}{\partial \overline{y}} + \overline{u_z} = 0 \tag{14}$$

where $\overline{h_p} = h_p/r_c$, $\overline{t} = t/t_c$, and we also replaced the seepage velocity $\overline{\mathbf{v}}$ by the average velocity $\overline{\mathbf{u}}$. This eliminates the porosity ε from the equation.

Finally we write the nondimensional boundary conditions for the pressure field, at the wetting front

$$\overline{p}|_{\overline{F}\,=\,0} = -1 \tag{15}$$

where the atmospheric pressure after nondimensionalization is negligible to be equal to 0. At the inlet contact area

$$\overline{p}\left(\overline{x},\overline{y},\overline{z},\overline{t}\right)|_{\overline{z}\,=\,0} = 0 \qquad \text{for } \overline{r} \le 1 \tag{16}$$

where $\overline{r} = r/r_c$.

A fundamental aspect of these nondimensional equations is that they are independent of any dimensionless number (Liu, 2017). In other words, the solution of nondimensional equations is independent of the contact radius r_c, the capillary pressure of inside of powder bed p_c, the permeability of the powder bed k or the effective pore radius r_{eff}, the viscosity μ, the surface tension of liquid γ or the contact angle θ between powder and liquid. In addition, we have shown that the penetration dynamic is also independent of the initial volume and initial radius of the sessile drop as well as the apparent contact angle between the drop and powder bed θ_a.

Under the assumptions and approximations discussed above, there exists a universal solution that applies to any powder-liquid system. It suggests that any quantity of interest can be given by a universal function of the dimensionless variables in the system. For example, the position of the wetting front h_p and corresponding volume of the wetted region V_s can be written as $h_p = r_c f\left(\overline{x},\overline{y},\overline{t}\right)$, and $V_s = {r_c}^3 g(\overline{t})$. Instead of expressing penetrated volume as a function of time, we can also write penetration time as a function

of volume. Note that penetrated volume of liquid $V_p(t) = \varepsilon V_s(t)$, and total penetrated volume $V_p\left(t = \tau_p\right) = V_0$. We can derive an expression for total penetration time τ_p,

$$\tau_p = t_c f_\tau\left(\overline{V}\right) = t_c f_\tau\left(\frac{V_p\left(t = \tau_p\right)}{\varepsilon {l_c}^3}\right) = \frac{\mu \varepsilon {r_c}^2}{k p_c} f_\tau\left(\frac{V_0}{\varepsilon {r_c}^3}\right) \tag{17}$$

for some universal function f_τ. We proved the a-priori non-trivial fact that, the penetration front dynamic is independent of the initial drop volume. Then, we can use the equation above to define the penetration time of an arbitrary nondimensional volume of fluid. For example, the penetration time τ_α for a penetrated volume of fluid equal to a fraction α of a hemisphere of radius r_c, $V_\alpha = \alpha(\frac{2}{3}\pi {r_c}^3)$, is expressed as

$$\tau_\alpha = \frac{\mu \varepsilon {r_c}^2}{k p_c} f_\tau\left(\frac{V_\alpha}{\varepsilon {r_c}^3}\right) = \frac{\mu \varepsilon {r_c}^2}{k p_c} f_\tau\left(\alpha \frac{2/3\pi}{\varepsilon}\right) \tag{18}$$

In the following section, we discuss how to take advantage of τ_α and corresponding intermediate penetrated volume to measure the contact angle for a powder-liquid system.

2.4 Contact angle measurements

In this section, we present a method to measure the contact angle of a given powder-liquid system subject to the discussions above (Liu, 2017). To this end, we assume that we have a *reference* liquid, with viscosity μ_R, surface tension γ_R, and most importantly, zero contact angle with the powder under consideration, which means complete wetting $\cos\theta_R = 1$.

Our goal is to determine the contact angle θ_T between a *test* liquid (viscosity μ_T, surface tension γ_T) with the same powder. The droplet penetration experiments including both reference and test liquids are performed on the same powder bed.

Based on Eqn. (18), we estimate the ratio of penetration times τ_α for both reference and test liquids

$$\frac{\tau_\alpha|_T}{\tau_\alpha|_R} = \frac{t_c|_T}{t_c|_R} = \left(\frac{\mu\varepsilon {r_c}^2}{kp_c}\right)_T \left(\frac{kp_c}{\mu\varepsilon {r_c}^2}\right)_R \tag{19}$$

Note that universal function f_τ cancels out because α is the same for both reference and test liquids. Plugging Eqn. (7) into the ratio, relying on the fact that for a same powder bed, permeability k, porosity ε, effective pore radius r_{eff} are the same in both cases.

$$\frac{\tau_\alpha|_T}{\tau_\alpha|_R} = \frac{\mu_T}{\mu_R}\left(\frac{r_c|_T}{r_c|_R}\right)^2 \frac{\gamma_R}{\gamma_T}\frac{1}{\cos\theta_T} \tag{20}$$

Rearranging the equation above, we obtain an expression of contact angle for test liquid as a function of two corresponding penetration times.

$$\cos\theta_T = \frac{\tau_\alpha|_R}{\tau_\alpha|_T}\frac{\mu_R}{\mu_T}\left(\frac{r_c|_R}{r_c|_T}\right)^2 \frac{\gamma_T}{\gamma_R} \tag{21}$$

The equation above has no explicit dependence on the transport properties of the powder bed. It is also clear to be independent of the actual solution to the penetration problem. In addition, we could repeat the calculation by selecting any dimensionless volume and corresponding penetration times for test and reference liquid obtained in experiments.

Chapter 3. Methodology & Experiments

3.1 Experimental Setup

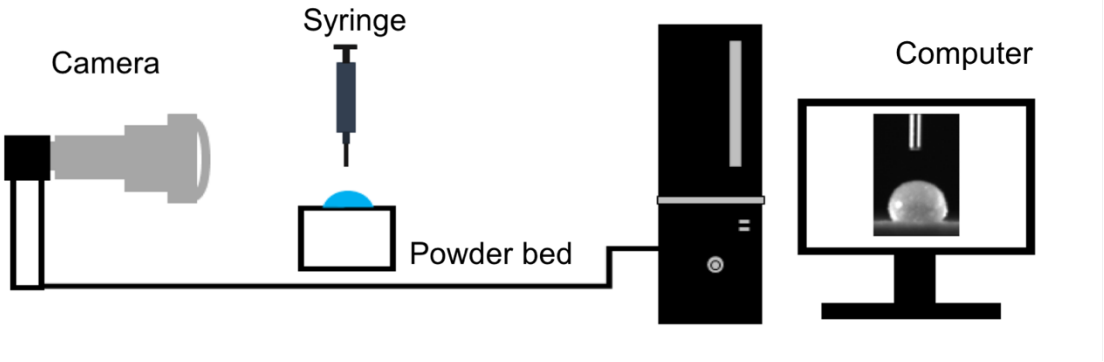

Fig 2 Schematic representation of droplet penetration experiment set-up

3.1.1 Setup

Figure 3.1 shows the scheme of our droplet penetration experimental set-up. Basically, a camera is connected to the computer to record the whole process of drop penetration on a slightly compressed powder bed. The powder bed is put on a height adjustable standing and right beneath the syringe.

There are two options to set the position of lights and result in different types of images. In the first choice, the camera, syringe and lights are kept on the same straight line with syringe in the middle. Then the shadow of drops are captured by the camera. The background is bright. As for another option, light is placed at two sides of the syringe and bed. So that the reflection of drops are captured by the camera. In this case the background is dark. We have experiments under both options to show both with good accuracy for analysis. Due to the convenience of editing movies afterwards, the first option was taken for most of the experiment results showed in this thesis.

After adjusting the position, focus and magnification of the camera, one can start recording and release the sessile drop from syringe gently by hand. The movie is saved by Streampix, a recording software from Norpix as an avi format video. There are two cameras with different maximum frame rates to select. The faster camera, Allied Vision Mako U029, is around 550 fps while the other one is around 60 fps.

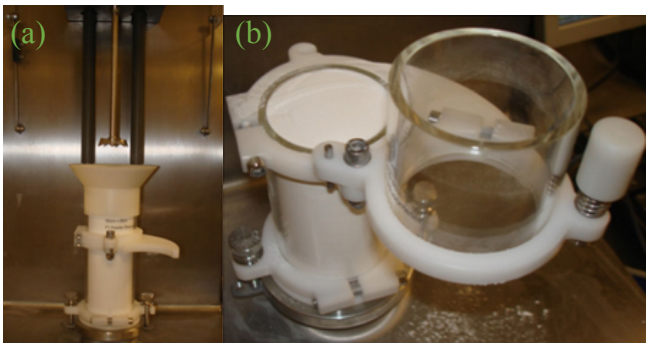

Fig 3 (a)Powder bed sitting on the FT4 machine; (b) powder bed after splitting.

3.1.2 Powder Bed and Surface

Freeman Technology 4 Powder Rheometer, FT4 for short, is used for preparing the powder bed and characterizing flowability of powder as well. Since there is no standard process preinstalled in the FT4 to prepare a slightly compressed powder bed, we choose one of the standard procedures, shear cell, to prepare the bed. The powder is placed into the split vessel which is the accessary of FT4. During the shear cell process, initial weight of powder put into the vessel is measured. Then several conditioning cycles are carried out to get rid of the effect of previous packing state of powder and make the packing more homogeneous. After conditioning, a vented piston compresses the powder bed until reaching a max constant pressure, usually 15kPa, which is the highest pressure in those preinstalled standard tests. The compressed powder column is cut into two parts by the

split vessel manually. Ideally a smooth surface could be obtained on top of the bottom part. The upper part of the vessel is removed from the powder bed. And then all the powders other than packed in the bed are collected in a plate. They are measured as split weight and used to calculate mass of the powder bed with initial weight. The volume of powder bed is a constant. We usually take the vessel of 10 ml and diameter of 25 mm. Hence the porosity of powder bed is easily determined.

The powder bed is placed underneath the syringe before any drop landing on its surface. The distance between tips and surface of beds should be adjusted accordingly. In our experiments PDMS and DI water drops releasing from the tip of same gauge is of different volume. Generally, the traveling distance between tips and the bed surface should be controlled around one half of the diameter of the corresponding sphere of the drop. Since a perfectly smooth powder surface is hardly observed, the selection of landing location on bed surface needs extra attention and patience. For example, in Fig. 4 the smooth surface is above the dash line, hence the bottom part below dash line should be avoided for depositing any drops. Sometimes, large area of smooth surface is hard to obtain especially for more cohesive powders.

Porosity of each powder bed is calculated by:

$$\varepsilon = 1 - \frac{m_1 - m_2}{\rho_T V_{bed}} \tag{22}$$

where m_1 is the initial mass of the powder added to the whole vessel, m_2 is the mass of powder collected after splitting the vessels, ρ_T is the total solid density of the material species and V_{bed} is the total volume of powder bed.

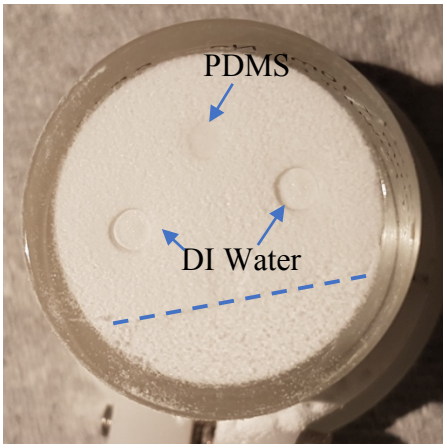

Fig. 4 Surface of a lactose powder bed with location of PDMS and DI water drops after penetration.

3.2 Analysis of Experiments

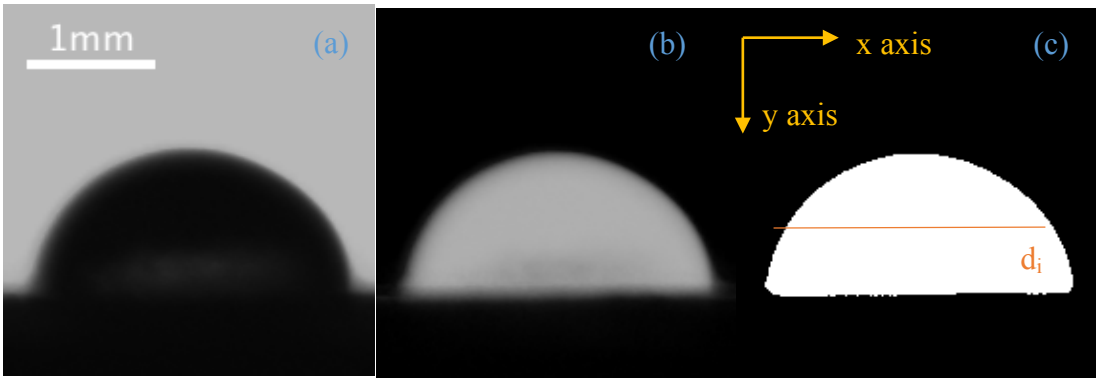

Fig 5 Example frame of a water drop penetrating into a lactose powder bed. (a) a frame before any editing; (b) invert color of the frame in (a) and subtract the background; (c) the frame in (b) after making binary.

3.2.1 Analysis of Frames

Penetration profile are extracted from the movies recorded by experiments. Hence editing and analysis of frames is required. Here we present an example of a water drop penetrating on lactose powder bed by using ImageJ. As showed in Fig 3.2.1, (a)(b)(c) is

the order of editing a single frame in the movie. From (a) to (b), the color is inverted and background is subtracted to make sure only desired drop left in the frame. From (b) to (c) the algorithm automatically picks a threshold through a function, usually we select default and then binarize the image keeping. The white part in (c) is the cross-section area of the water drop. Next, the algorithm to calculate volume from the area is presented.

The drop is assumed to be axisymmetric. Imaging in (c), we cut the drop along the x-axis into multiple thin plates with thickness of one pixel perpendicular to the y-axis. The drop volume is calculated by the sum of these thin cylindrical plates, as Eqn. (23). n is the total number of plates. h is the thickness of each plate. d_i is the diameter of plate #i.

$$V = \sum_{i=1}^{n} \frac{\pi}{4} d_i^2 * h \qquad (23)$$

As the quality of the image at the bottom part of the drop is not always perfect, the diameter of the contact area between drop and the porous bed is recognized by the longest diameter of those plates mentioned before. However, if the apparent contact angle is smaller than 90 degree, the result will bring errors. To deal with this situation, we match the longest plates with its y coordinate. If the y value obviously departs from the y coordinate of the bed surface, then for this frame we can claim that the measurement cannot be trusted. Fortunately, in most of the frames other than bouncing stage at the beginning, the apparent contact angle between drop and powder surface is larger than 90 degree. These observations are based on the experiments of DI water and PDMS drops. As a result, we can observe the change of contact area radius with time of penetration.

Penetration profile, drop volume vs time, is obtained by the plugin macro in ImageJ written based on the algorithm mentioned before. The profile with units of pixel then transferred to corresponding real length scale latter in Excel sheet.

We also notice the periodic fluctuation on curves with longer penetration time, especially when using the higher speed camera. The unexpected phenomena are due to the slightly vibration of the stand of camera. We could eliminate it by adding vibration isolation equipment to our setups.

3.2.2 Calculation of Contact Angle

We need to determine the initial volume and constant contact radius from the penetration profile. These two parameters are essential to the further analysis to determine contact angle. For initial volume, I plot the penetration profile from first frame that drop just touch the surface to the end that drop completely disappears. Then select the largest volume in which point the volume starts to decrease steadily as the initial volume and the corresponding time point as the zero point of adsorption time. In almost all the cases there is a rapid bouncing, fluctuation or lose of volume in a few frames at beginning. We assume that the penetration process we are interested in takes place at the end of the unsteady phase.

Constant contact radius is determined form the plot of contact radius vs time. This constant is handpicked as an average value through a certain time with more or less constant radius. Contact radius always shrinks to zero rapidly near the end of the penetration due to the disappearance of drop and relatively low image quality at the edge of bed surface.

$$V_p = V_0 - V \tag{24}$$

$$\widehat{V_p} = \frac{V_p}{\frac{2}{3}\pi r_c^3} \tag{25}$$

Penetrated volume V_p means the volume of drop has already penetrated into the powder bed. It is calculated by V_0 , initial volume and volume of drop, V, measured by ImageJ through Eqn. (24). Non-dimensional volume is calculated by Eqn. (25), penetrated volume divided by volume of semi-sphere whose radius is the picked constant contact radius.

$$\hat{t} = \frac{2k}{r_{eff}} \frac{1}{r_c^2} \frac{\gamma_{lv}}{\mu\varepsilon} \cos\theta * t \tag{26}$$

Based on Darcy's Law, non-dimensional time can be expressed in Eqn. (26). However, we don't know the permeability k for the powder bed, capillary pore radius r_{eff}, and cosine contact angle.

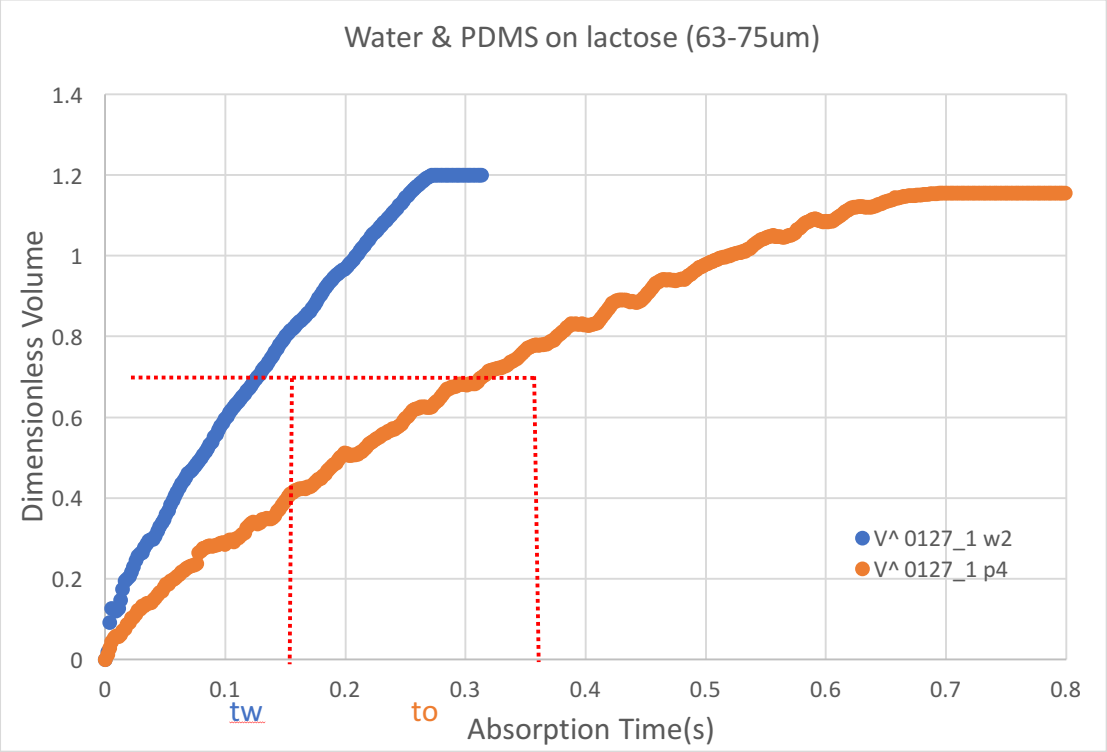

Fig 6

What we are interested now is the contact angle between water and powder. PDMS is taken as a reference liquid, which is of low surface tension to decouple the effect of

porous powder bed. Once we obtain the ratio of two cosine value of contact angle by Eqn. (27), we assume contact angle of PDMS between powder bed is 0 degree. Then the contact angle of water is determined by the ratio.

$$\frac{\cos\theta_w}{\cos\theta_o} = \frac{t_o}{t_w}\left(\frac{r_w}{r_o}\right)^2 \cdot \frac{\gamma_o}{\gamma_w} \cdot \frac{\mu_w}{\mu_o} \tag{27}$$

Multiple nondimensional volume can be chosen and consequently calculate corresponding contact angle. However, the penetration profile obtained by analysis of movie is not a continuous variation with time. Hence, linear interpolation was used to transfer discrete profile into a continuous volume profile with variation of time. However, the use of linear interpolation could bring errors to our results, especially in the initial stage, when there is much less discrete points to be based on for interpolation than later stage. Because there is relatively faster decrease of drop volume in initial stage than later in all profiles obtained from experiments.

3.3 Materials

The properties of powder materials and liquids used in our experiments is presented below

Powder Material	Chemical Formula	Raw material particle size distribution d50 (um)
Lactose Monohydrate	$C_{12}H_{24}O_{12}$	60
Caffeine Anhydrous	$C_8H_{10}N_4O_2$	30

	Liquid	Viscosity (cst) (T = 20 °C)	Surface tension (mN/m) (T = 20 °C)
Tested Liquid	Deionized Water	1	72.1
Reference Liquid	Silicone Oil	10	20.1

Chapter 4. Results of Lactose Powder

We will discuss some experimental results about lactose powder in this chapter. We used lactose monohydrate with regular grind manufactured by Foremost Farm USA. The particle size distribution of the raw material in the drum is characterized by d50 value equal to 60um. Particle size distribution was measured using a Laser Diffraction Spectroscopy technique (Beckman-Coulter LS 13 320 series laser diffraction particle size analyzer). We carried out droplet penetration experiments on several groups of lactose powder separated by particle size distribution. The separation was fulfilled by sieving. The size of mesh at the top is 106um. Material was collected from meshes: 90um, 75um, 63um,53um, 45um and 38um.

Each powder with different particle size distribution will be named as the mesh size from which they collected from in the rest of the thesis. For example, powder with particle size 90~106 um will be named as 90 um powder.

Particle Size(um)	Permeability (*10^9 cm^2)
90~106	9.08
75~90	17.06
63~75	21.18
53~63	29.95
45~53	47.28
38~45	55.11

The procedures of making powder bed for the test is the same as in drop penetration method. The maximum normal pressure compressing the powder is 15kPa.

The variation of porosity is shown in Fig 7. There are 3 powder beds made and measured porosity in each particle size distribution. Except the relatively large error bar in the range of 75~90um, the porosity is decreasing with the increasing of particle. The trend can be explained as the effect of cohesive lactose powder, since the cohesive force rises as the particle size goes down. A larger cohesive force will result in a larger porosity under same normal pressure.

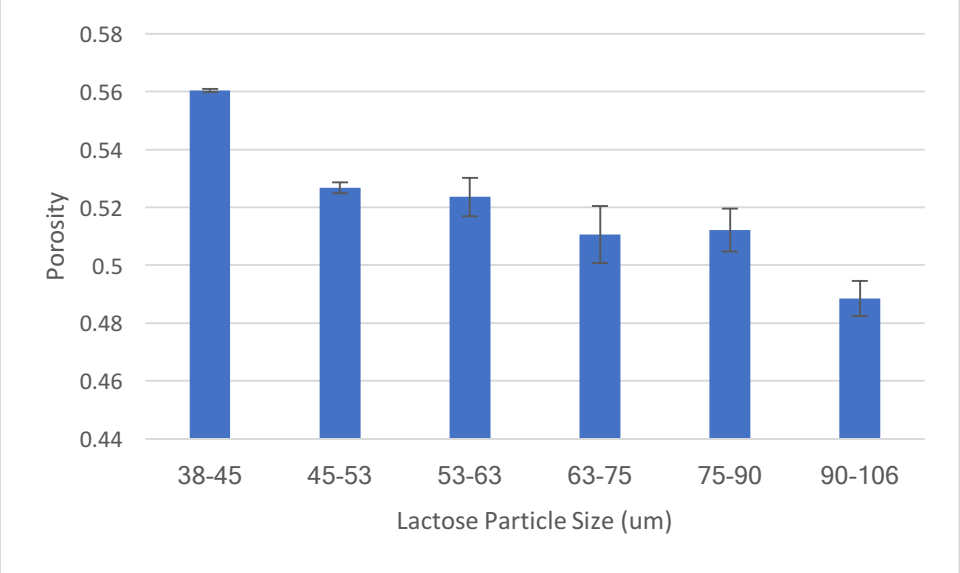

Fig 7 Porosity vs particle size distribution of lactose.

Permeability test of lactose powders with various particle size were carried out by FT4. According to the well-known Kozeny-Carman Equation (Carman, 1956), the permeability is proportional to the square of the diameter of spherical particles, given that porosity is uniform. We neglect the variation in the porosity of packed powder beds with different particle size distribution and approximate the lower size border as the diameter of particles. For example, the diameter of lactose powder with size range 38~45um is

approximated as 38um. As shown in Fig 8, we found that the permeability of lactose powder bed could also be approximately proportional to the square of particle diameter.

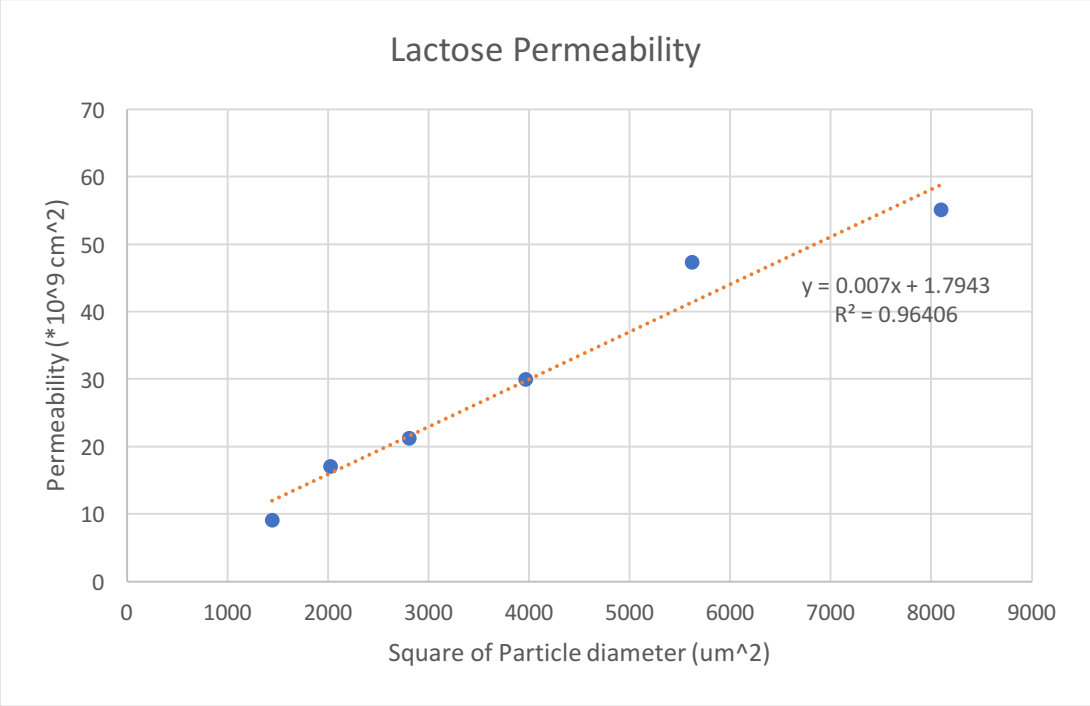

Fig 8 Permeability of lactose vs square of lower particle size border.

As mentioned in Chapter 3, deionized water is the testing liquid and silicone oil with viscosity of 10cst is the reference liquid in our droplet penetration experiments. we can first plot the change of contact region radius with time, which is shown in Fig 9.

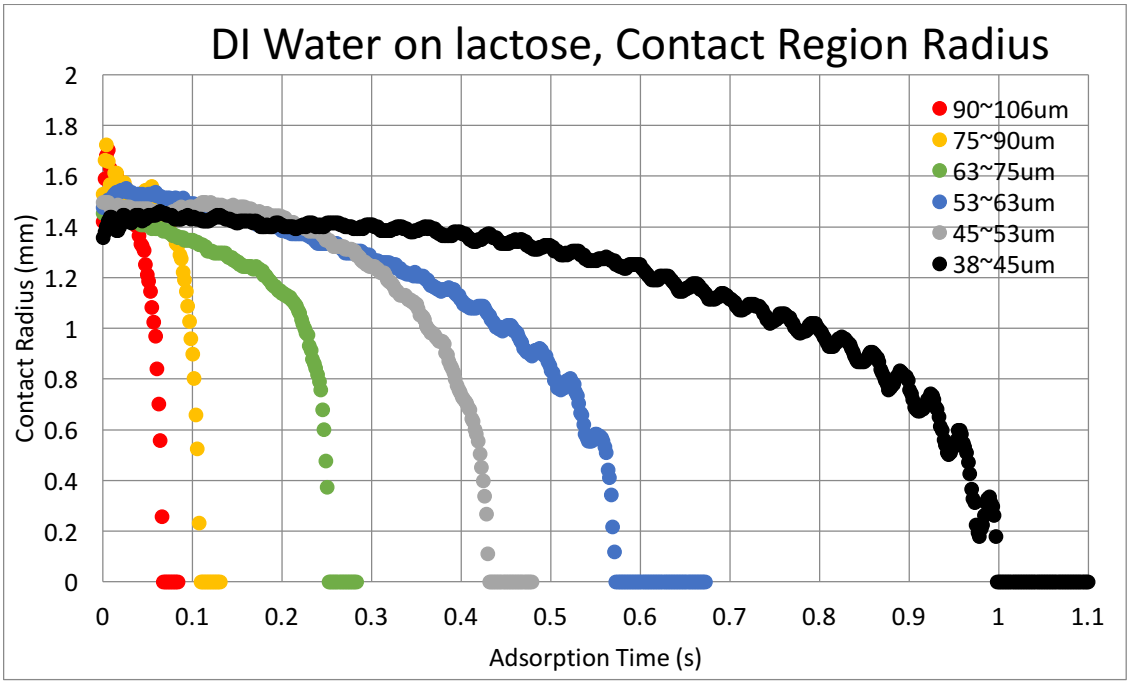
DI Water on lactose, Contact Region Radius
Contact Radius (mm)
Adsorption Time (s)
90~106um
75~90um
63~75um
53~63um
45~53um
38~45um
0
0.2
0.4
0.6
0.8
1
1.2
1.4
1.6
1.8
2
0
0.1
0.2
0.3
0.4
0.5
0.6
0.7
0.8
0.9
1
1.1

(a)

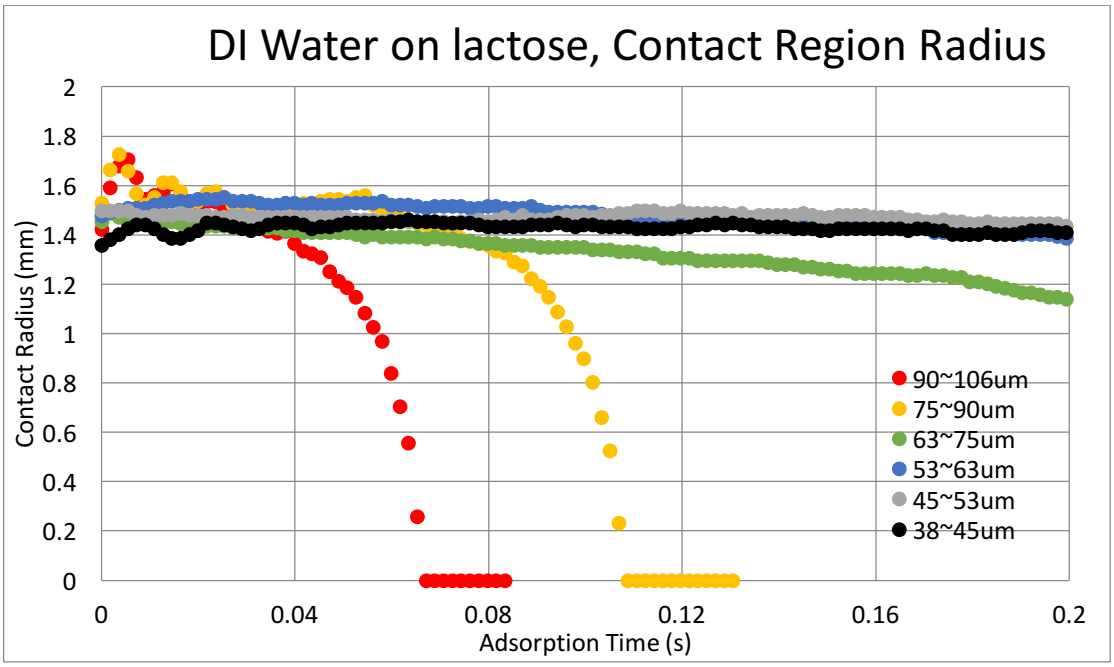
DI Water on lactose, Contact Region Radius
Contact Radius (mm)
Adsorption Time (s)
90~106um
75~90um
63~75um
53~63um
45~53um
38~45um
0
0.2
0.4
0.6
0.8
1
1.2
1.4
1.6
1.8
2
0
0.04
0.08
0.12
0.16
0.2

(b)

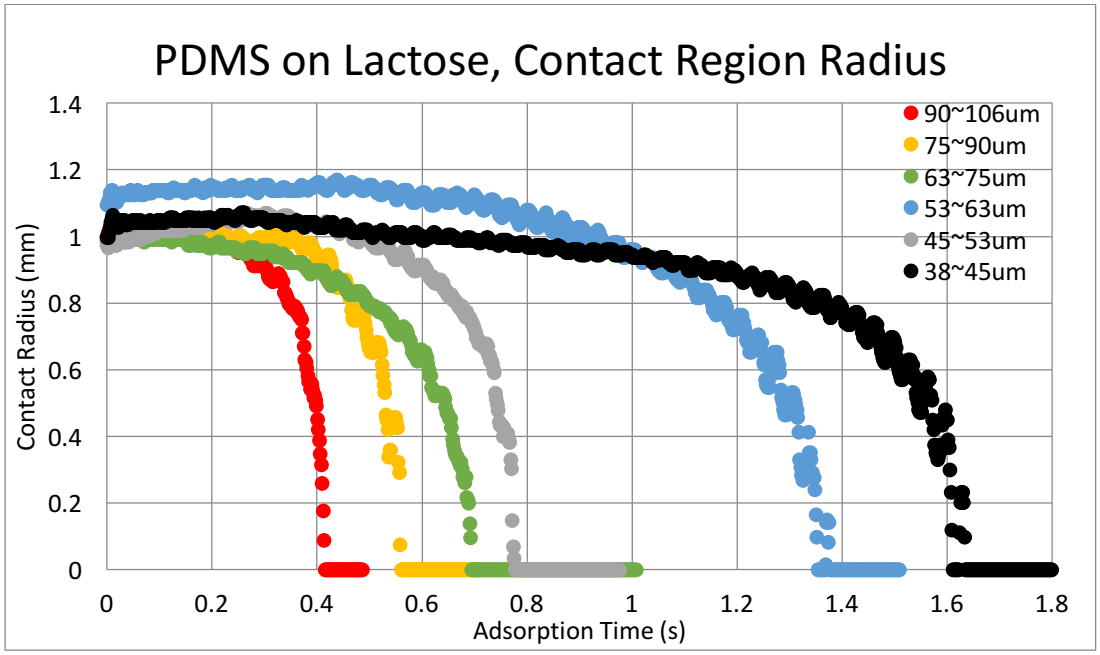

(c)

Fig 9 (a) DI water penetrated on lactose beds with 6 groups of different particle size distribution. (b) Zoom in of (a) at short time. (c) PDMS penetrated on the same bed as DI water.

In our model, the penetration is expected to take place at a constant contact area. The results above show that the radius of the droplet sitting on the porous bed can be well approximated by a constant during large part of the experiments and for both liquids. Therefore, CDA (constant drawing area) assumption can be considered valid. We shall determine a constant contact radius as the characteristic penetration length r_c based on plots above. Note that PDMS has a longer relative period of constant radius than DI water in all the 6 groups on lactose powder bed. Recall the discussion of Denesuk et al. (Denesuk M. Z., 1994), it could suggest that the ratio of spreading time over penetration time for PDMS drops is smaller than the ratio for DI water.

The results of penetration profiles, droplet volume vs time, are shown as in Fig 10. If there is a bouncing stage at the beginning of volume profile, the value of the last peak point was selected as the initial volume. Then, we can convert droplet volume into volume of liquid already penetrated into the powder bed as Eqn. (24). The variation of penetrated volume with adsorption time, which is reset as we put the corresponding time of initial volume as zero time point, was presented in Fig 11.

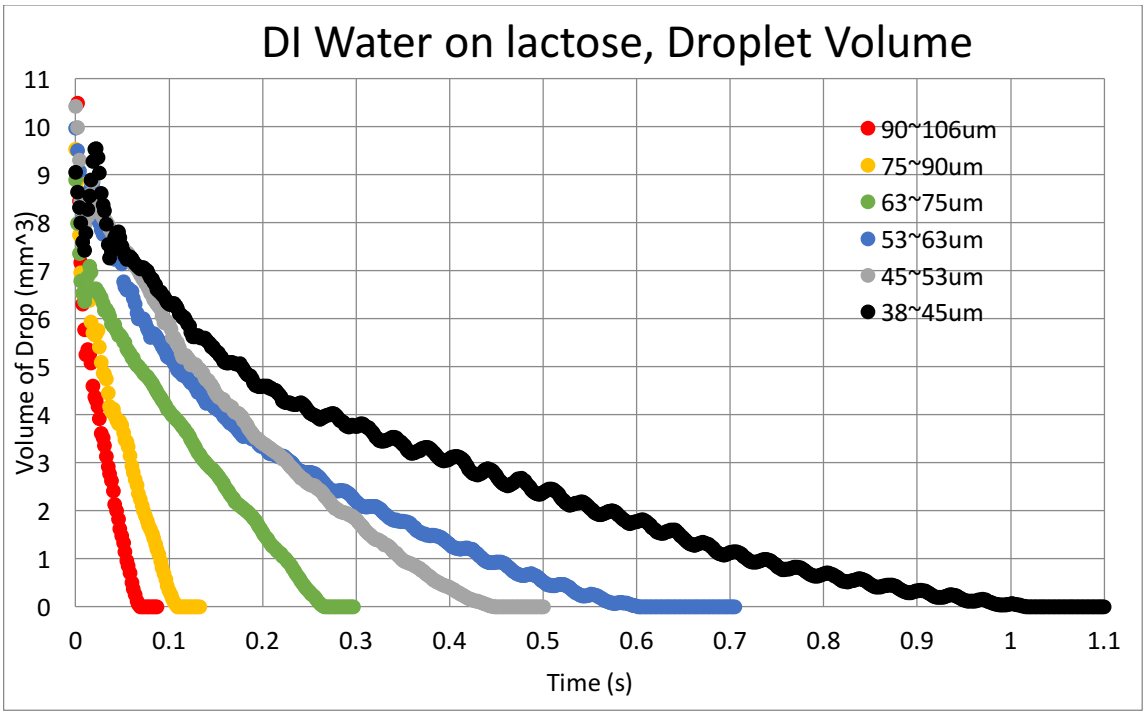

(a)

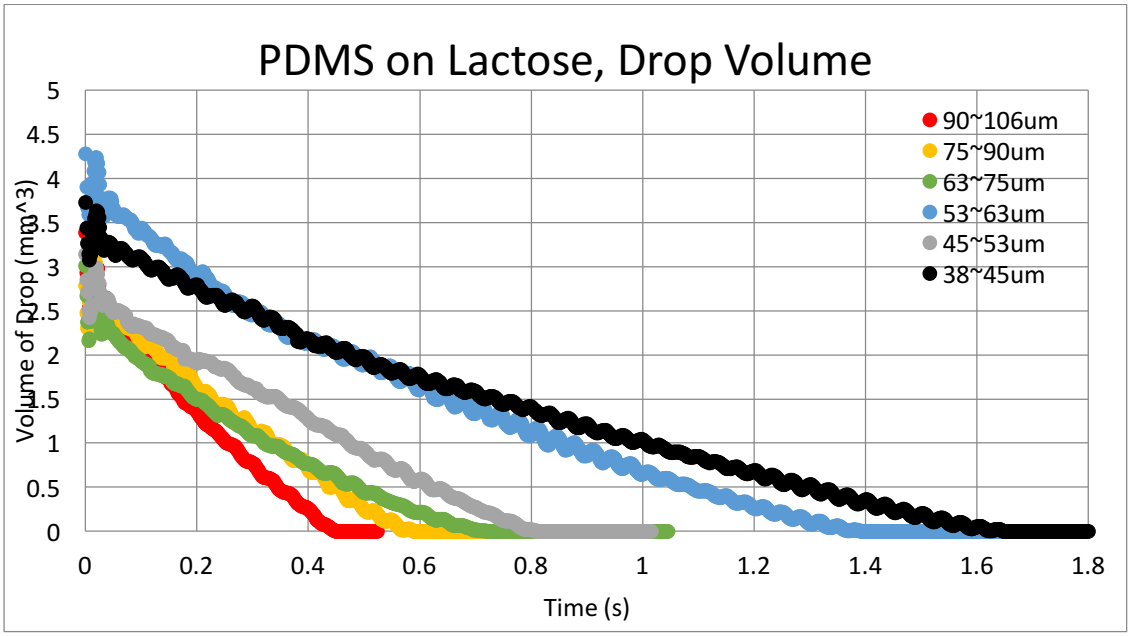

(b)

Fig 10 (a) DI water drop penetration on lactose with 6 groups of different particle size distribution. (b) PDMS drop penetration on the same beds as in (a).

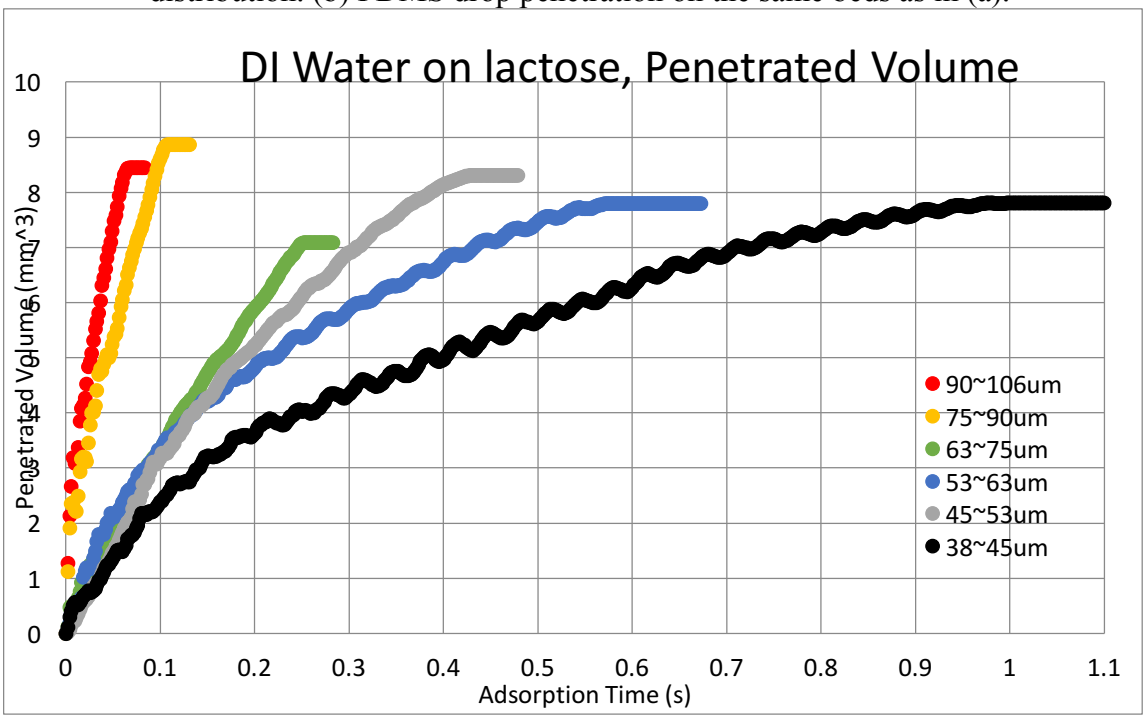

(a)

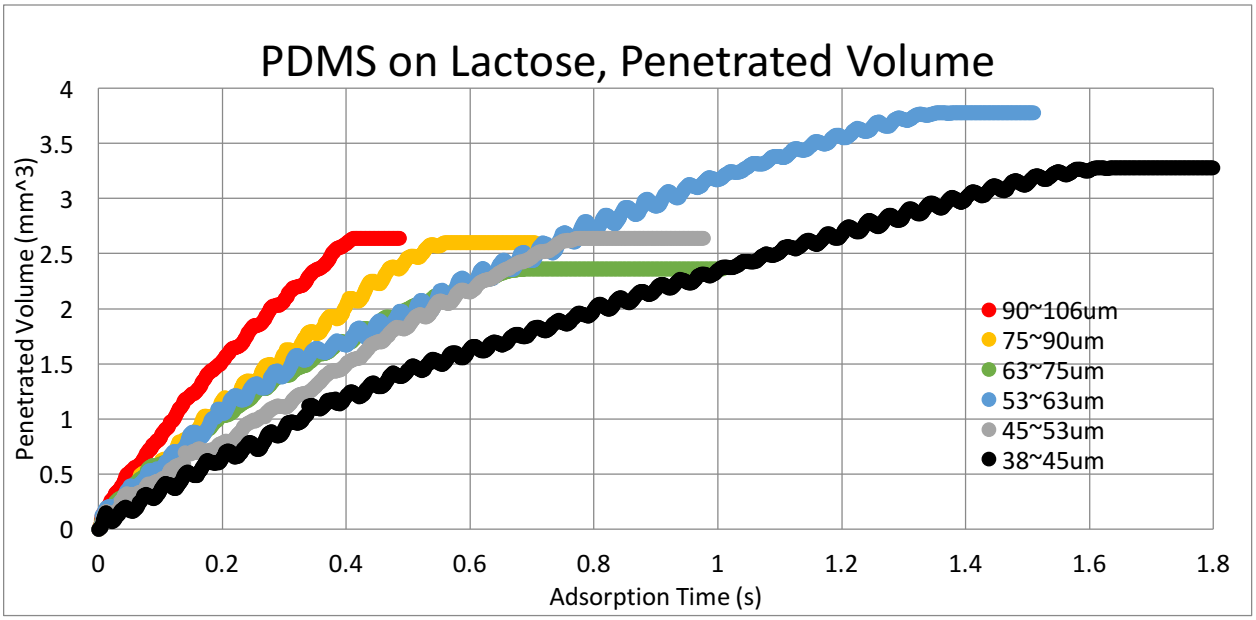

(b)

Fig 11 penetration volume of DI water on lactose with 6 groups of different particle size distribution. (b) PDMS drop penetration on the same beds as in (a).

It is clear that the total penetration time of both different liquids varies significantly with the particle size distribution of each group. Specifically, the total penetration time increases with the decreasing of particle size, for both DI water and PDMS, excluding the 53um powder. With a similar initial volume, this suggests that the rate of penetration on lactose powder bed of both liquids also varies significantly and is decreasing with the decreasing of particle size.

When comparing two liquids, the total penetration time of DI water drop is shorter than PDMS drop on the same lactose powder bed, despite that the initial volume of water drop is approximately three times to PDMS drop's.

We would like to check if the receding occurs at the same apparent contact angle for lactose with different particle size distribution. After determining r_c we can plot nondimensional contact radius r/r_c vs corresponding cosine of apparent contact angle as shown in Fig 12. We assume that the shape of drop in our movies is part of a sphere. The effect of gravity on drop shape and receding behavior is neglected. Then apparent contact angle θ_a could be calculated as:

$$\cos\theta_a = \frac{r^2 - h^2}{r^2 + h^2} \tag{28}$$

where r is the contact region radius, h is the height of the drop.

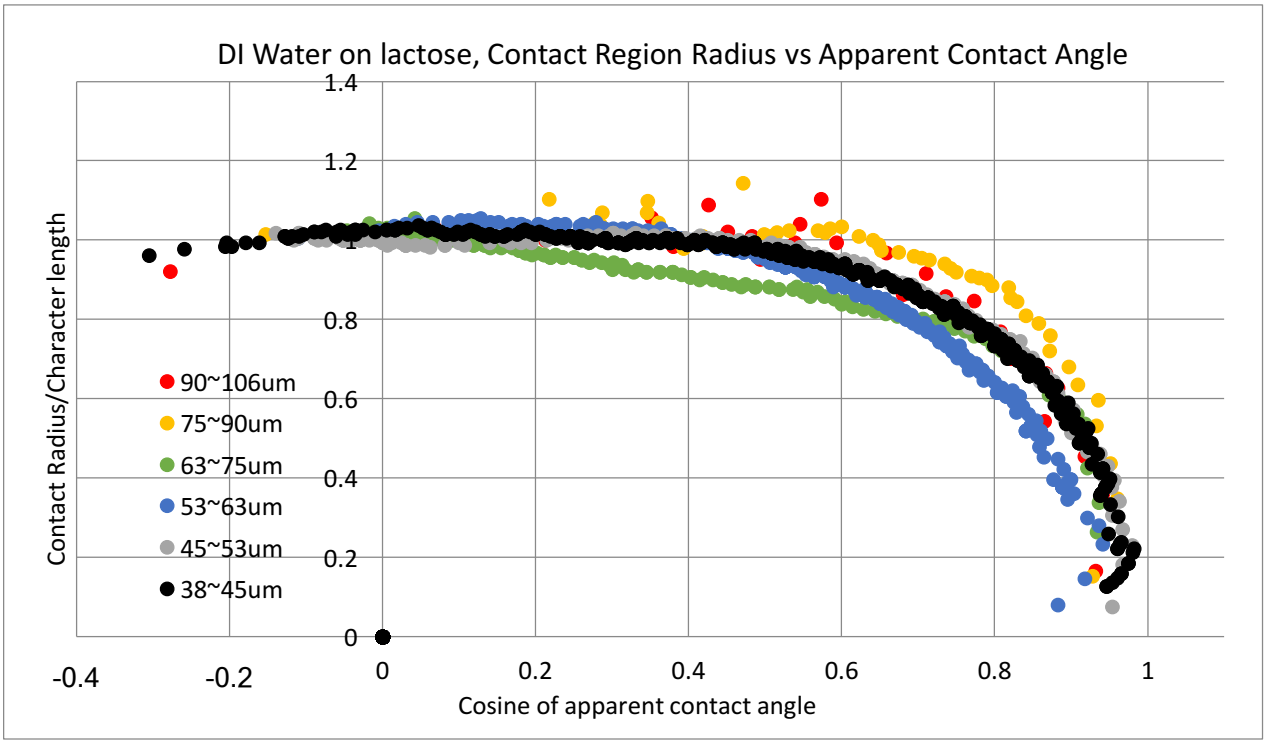

(a)

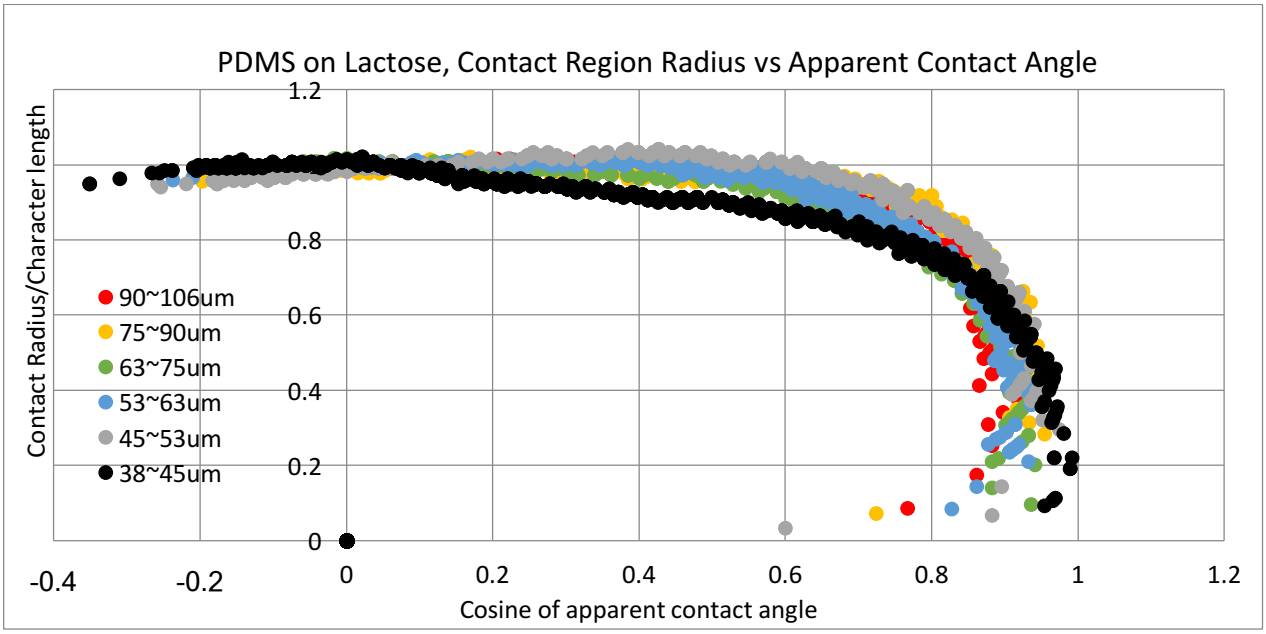

(b)

Fig 12 Nondimensional radius of contact between the droplet and the powder bed vs cosine of apparent contact angel. (a) DI water penetrated on lactose beds with 6 groups of different particle size distribution. (b) PDMS penetrated on the same bed as DI water.

For both cases of DI water and PDMS, curves from 6 groups appear to be overlapping. Considering the accuracy of our recording, we could draw the conclusion that particle size distribution has little effect on the receding behavior of both DI water and PDMS drops while penetrating on lactose powder bed.

Next, we shall take a look at the nondimensional plots, which is nondimensional volume vs nondimensional time. For penetrated volume we, use Eqn. (25) to make it nondimensional. However, for nondimensional time $\bar{t}$, we are incapable of directly measuring the permeability k, effective pore size r_{eff} and contact angle θ inside the powder bed. Therefore, without a known r_{eff} and local permeability for liquids, it is impractical to estimate t_c as Eqn. (11) and $\bar{t} = t/t_c$ as well. However, we can still define t^*as:

$$t^* = t\frac{\gamma}{\mu {r_c}^2 \varepsilon} 4k_{air}/d_p \cong \bar{t}/_{cos\theta} \quad (29)$$

Note that t is the adsorption time, k_{air} is the air permeability measured in experiments and d_p is the center diameter value of particle size distribution. For example, for the particle size of 90~106 um, d_p = 98 um. Then we plotted nondimensional wetted volume vs t^* for DI water and PDMS drops respectively as shown in Fig 13.

In our theory described in Chapter 2, we expected that plots of nondimensional volume vs $\bar{t}$ are overlapping among any different liquids penetrating on any powder beds as long as our assumptions and approximations valid. We took t^* as an approximation to the nondimensional time over cosine contact angle, $\bar{t}/_{cos\theta}$. Then, if the contact angle of the same liquid on powder beds is independent of the powder particle size distribution, we also expected to see overlapping among nondimensional volume vs t^* profiles with different particle size distribution. The overlapping among profiles of PDMS is exactly what we saw in Fig 13 (b). It suggested that the contact angle of PDMS on lactose powder bed doesn't shift with the variation of powder particle size distribution. In addition, the PDMS is of low surface tension and expected to have small contact angle. Therefore, PDMS could be used as a reference liquid with an assumption that the contact angle equals to 0° . The overlapping of different profiles also indicated the existence of an universal function connecting nondimensional volume and time as described in the Chapter 2.

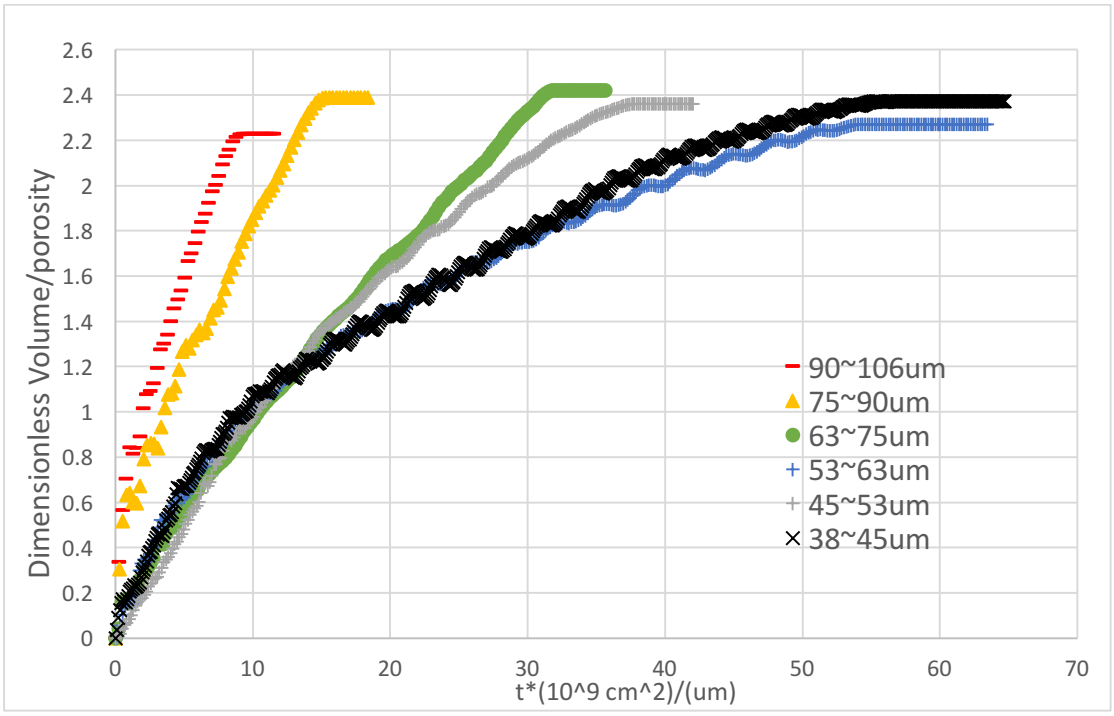
Dimensionless Volume/porosity
t*(10^9 cm^2)/(um)
90~106um
75~90um
63~75um
53~63um
45~53um
38~45um

(a)

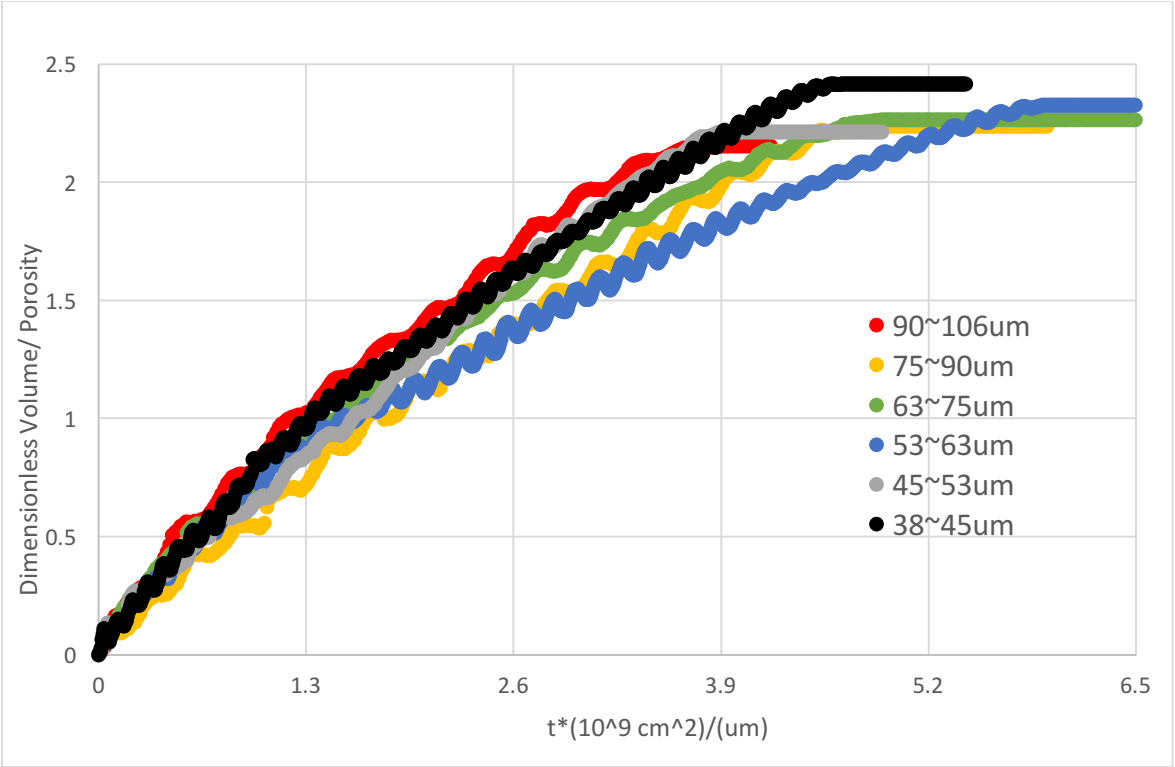
Dimensionless Volume/ Porosity
t*(10^9 cm^2)/(um)
90~106um
75~90um
63~75um
53~63um
45~53um
38~45um

(b)

Fig 13 (a) DI water and (b) PDMS nondimensional penetration profile on lactose powder beds of different particle size distribution, respectively.

However, in the case of water, the situation is more complicated. The four profiles with smaller powder particle size distribution from 38 to 63um are overlapping at the early stage for a significant amount of nondimensional wetted region volume, yet separated from the larger two sizes, 75um and 90um. It could suggest that the contact angle of two larger particle size, 75um and 90um, is larger than the rest four smaller lactose powder particle size distributions.

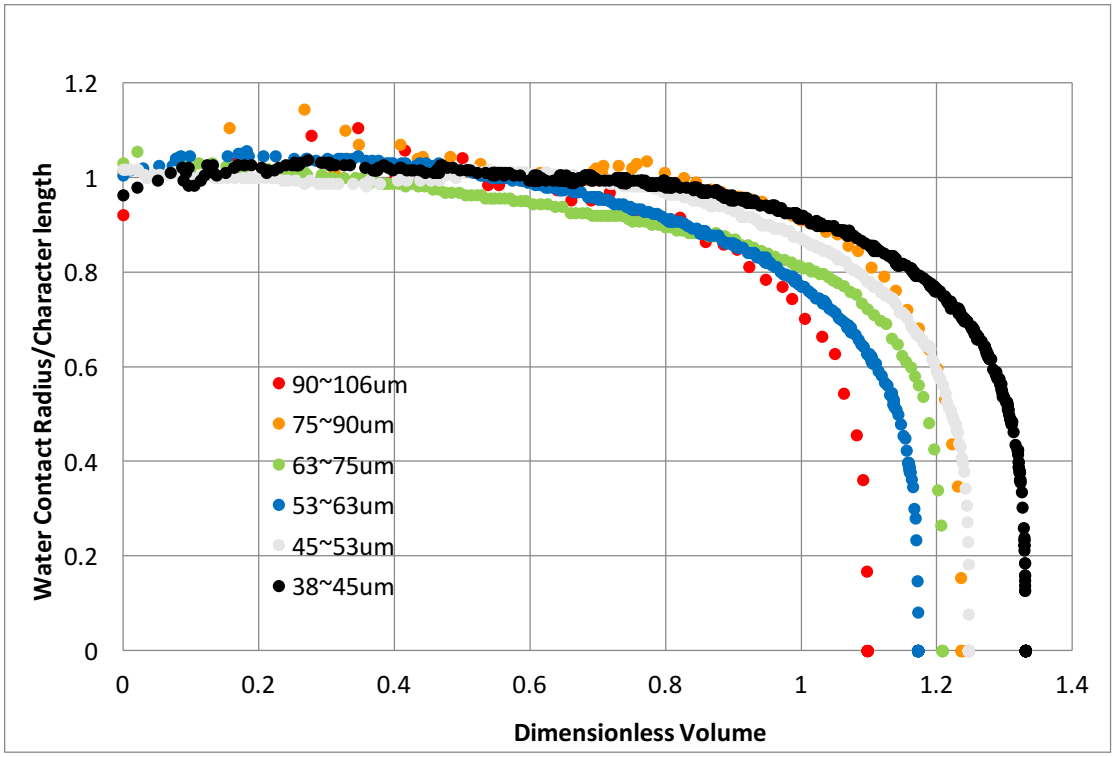

(a)

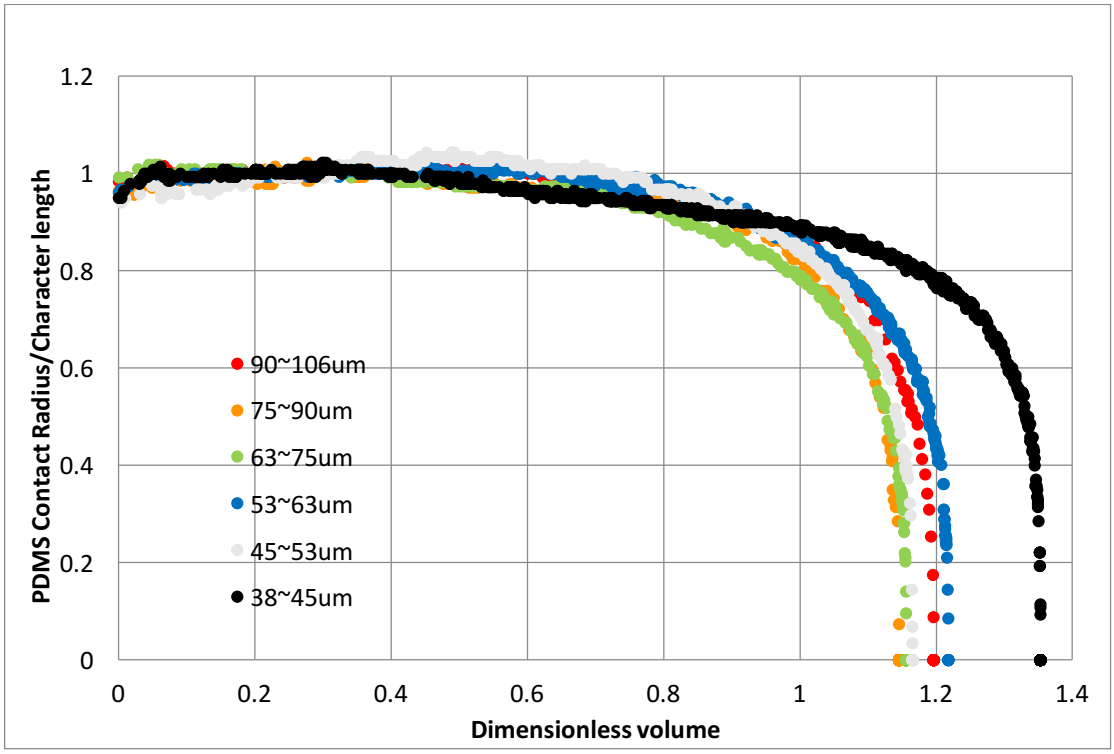

(b)

Fig. 14 Nondimensional contact radius vs dimensionless volume. (a)DI Water (b)PDMS with different lactose powder bed particle size distribution.

As mentioned in Chapter 2, we are able to use multiple nondimensional volumes and corresponding adsorption time to determine the value of cosine contact angle. The range of dimensionless volume that can yield results as accurate as possible had to be determined. To this end, we plotted nondimensional contact radius vs dimensionless volume for each particle size and liquid drop to estimate the range of dimensionless volume in which CDA approximation is valid. For both liquids, the CDA is approximately valid in the range of dimensionless volume from 0.2 to 0.8.

Finally, we present some results on calculated contact angle.

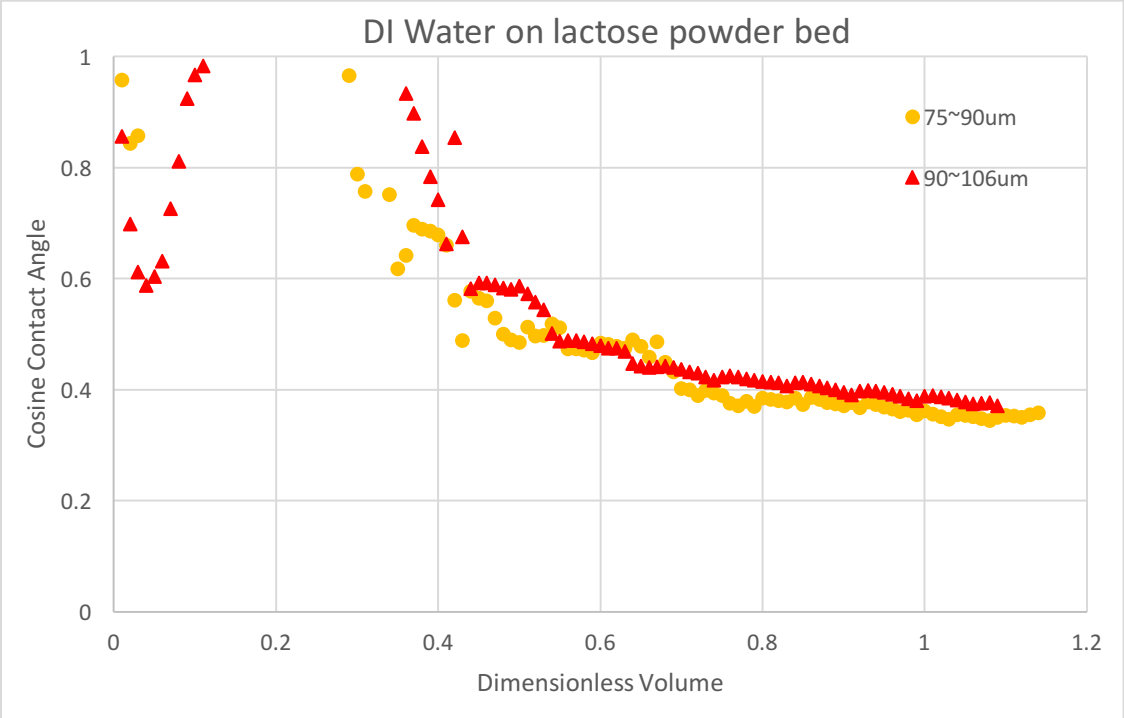

(a)

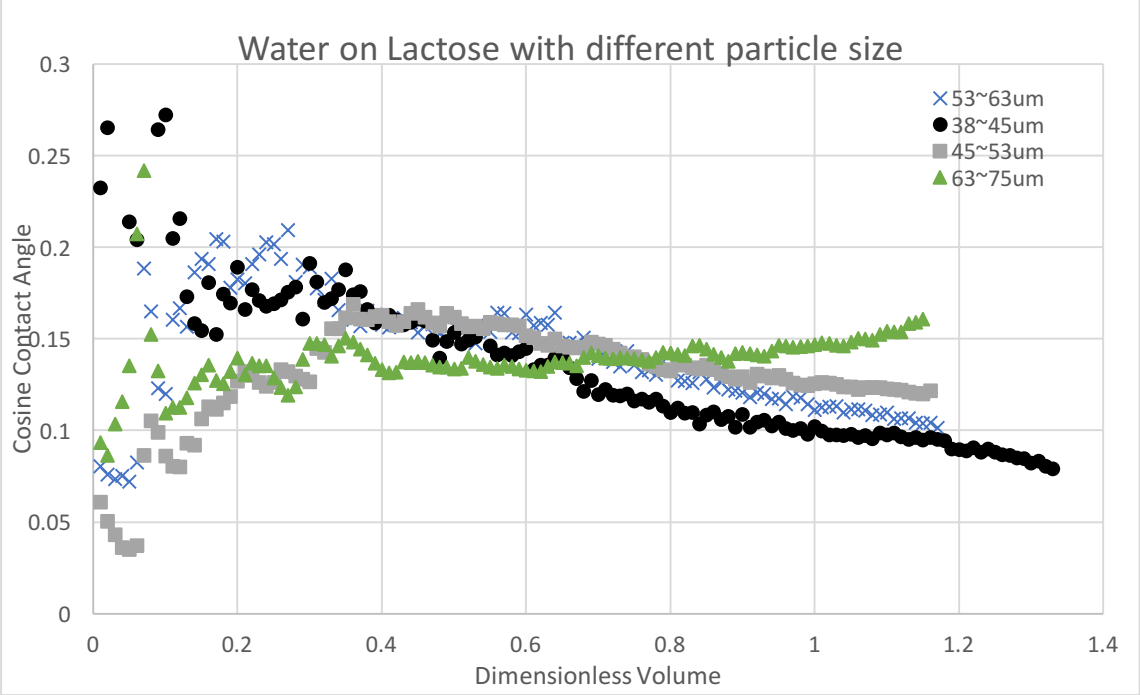

(b)

Fig 15 Cosine contact angle vs Dimensionless Volume of DI water on lactose with various particle size

From Fig 15 (a) and (b), the cosine contact angle changed dramatically at small nondimensional volume. Part of the reasons of these phenomena are the interpolation used in obtaining corresponding time for each nondimensional volume as mentioned in Chapter 3. Except the two largest particle size, which has a dramatic decrease in drop volume at initial stage, most curves in these figures tend to stabilize after certain point, say nondimensional volume = 0.2. Different selection of nondimensional volume ends in the similar cosine contact angle demonstrate our method valid.

Comparing Fig 15 (a) and (b), we can see a jump of cosine contact angle. According to a reference (Depalo, 2013) the cosine contact angle between lactose and water is around 0.15 at 20 °C. Average cosine contact angle from three different segment of dimensionless volume, 0.21~0.4, 0.41~0.6, 0.61~0.8. is plotted below. For lactose powder, the contact angle of water is independent of powder particle size distribution if the size is smaller than 75um.And the cosine contact angle is close to the reference.

The average over nondimensional value 0.21~0.4 and 0.41~0.6 for the cases of two larger particle size are not present below. Because the value is beyond 1 and those are not acceptable as reasonable results. Other than that, The average of powder bed with particle size 75um and 90um is much higher than the refernce value. It could suggest that a faster camera is needed to capture the relatively faster penetration process in the case of these two larger size lactose. And our theory might not be working appropriately in these cases.

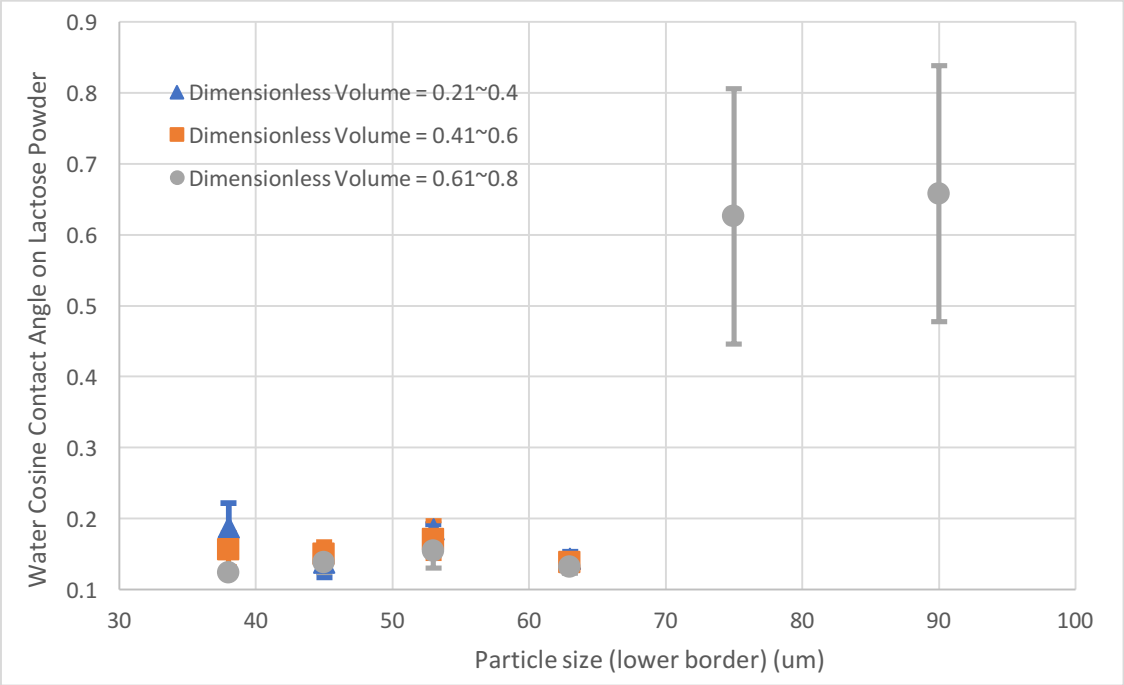

Fig 16 Average of cosine contact angle over nondimensional volume 0.21~0.4, 0.41~0.6, 0.61~0.8.

Chapter 5. Results of Caffeine Powder

In this chapter, we shall discuss some results of experiments and analysis with powder beds made up of caffeine. The raw material is caffeine anhydrous manufactured by CSPC Innovation Pharmaceutical Co, Ltd.

As we did in the case of lactose, we tried to investigate the effect of particle size on the wettability of caffeine. That's been said, we didn't use sieving as the experimental method to separate groups of caffeine with different size distribution. Instead, we milled the raw material, which has a size distribution of d50 number approximately equal to 30 microns, by jet milling.

The mechanism of jet milling is to break the caffeine crystal particles by collisions between two particles of high speed or between single particle and walls. The acceleration of particles is driven by high pressure air flow. There are three parameters, feed rate, feed pressure and grinding pressure, for the jet miller to control the final particle distribution of fine powder. Feed rate is the amount of powder per time added to the grinding chamber. Feed pressure is the pressure of the air flow carrying powder into the grinding chamber. Grinding pressure is the pressure of air flow driving the grinding process happened in the metal chamber. The table below shows the results of caffeine powder groups of different particle size distribution and their corresponding milling parameters. The last column in the table is the corresponding porosity of caffeine powder bed measured in our drop penetration experiments with a maximum normal pressure at 15kPa.

D50 of particle size distribution (um)	Feed rate	Feed pressure (psi)	Grinding Pressure (psi)	Average Porosity (normal pressure =15kpa)
30	0	0	0	0.44
19	900	10	10	0.45
15	900	20	20	0.59
5	600	30	30	0.69

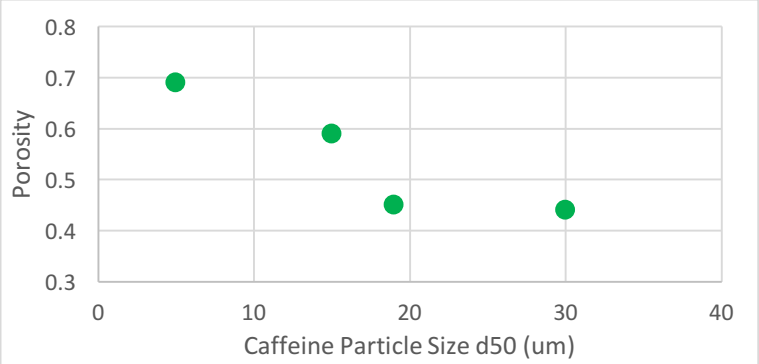

Fig. 17 Caffeine porosity vs particle size. Applied normal pressure = 15 kPa

Next we shall present some examples of penetration profiles on caffeine powder.

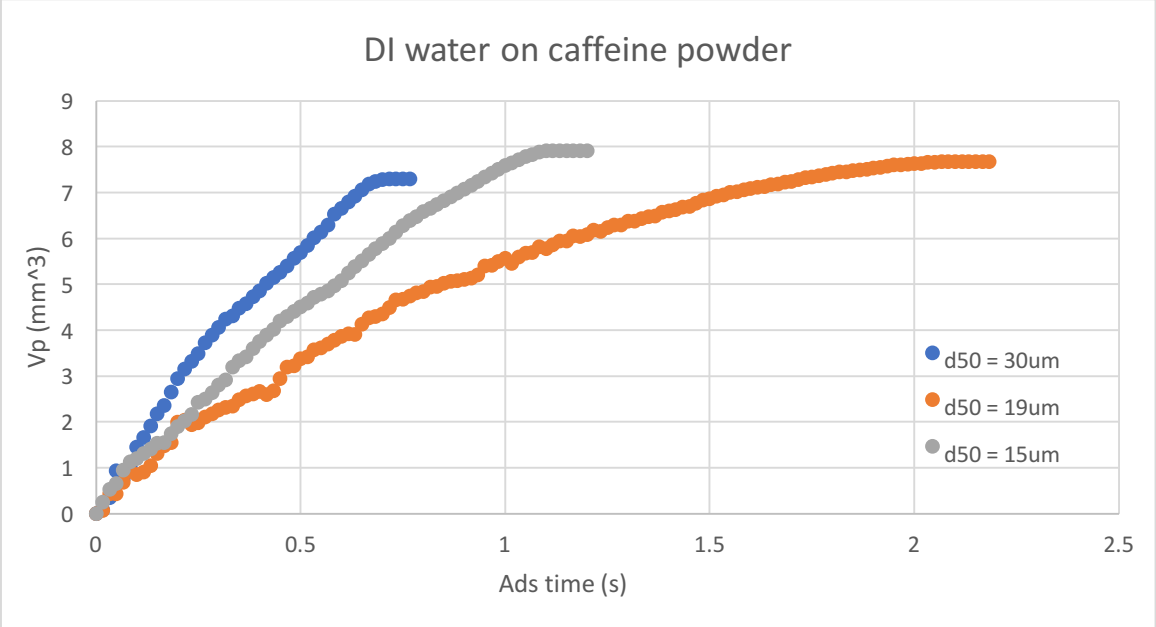

(a)

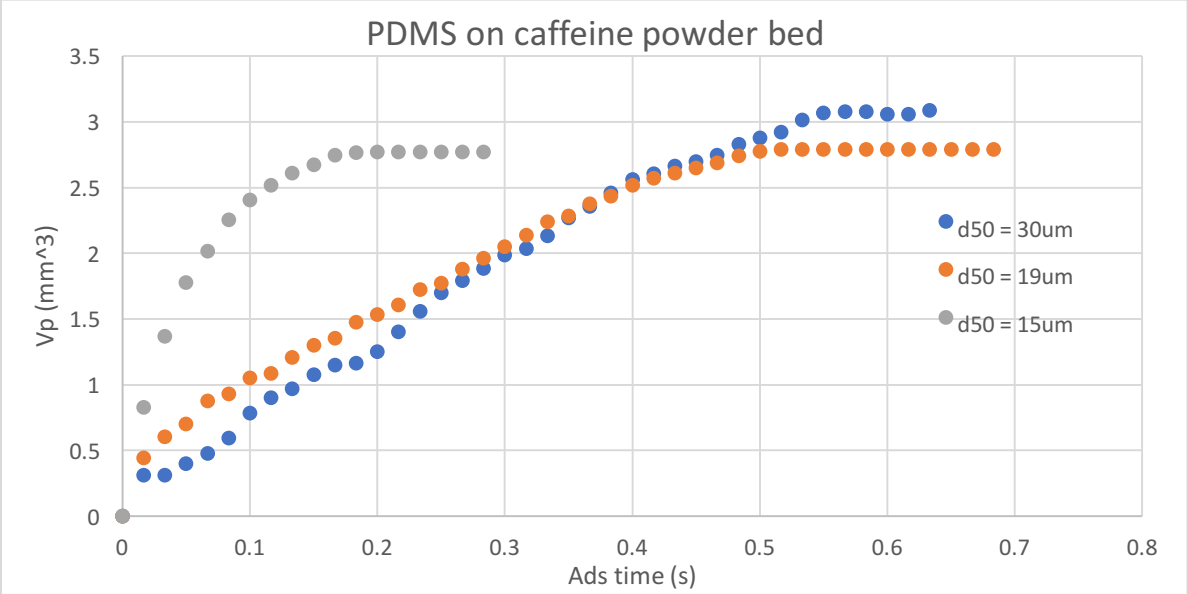
PDMS on caffeine powder bed
Vp (mm^3)
Ads time (s)
d50 = 30um
d50 = 19um
d50 = 15um
0
0.5
1
1.5
2
2.5
3
3.5
0.1
0.2
0.3
0.4
0.5
0.6
0.7
0.8

(b)

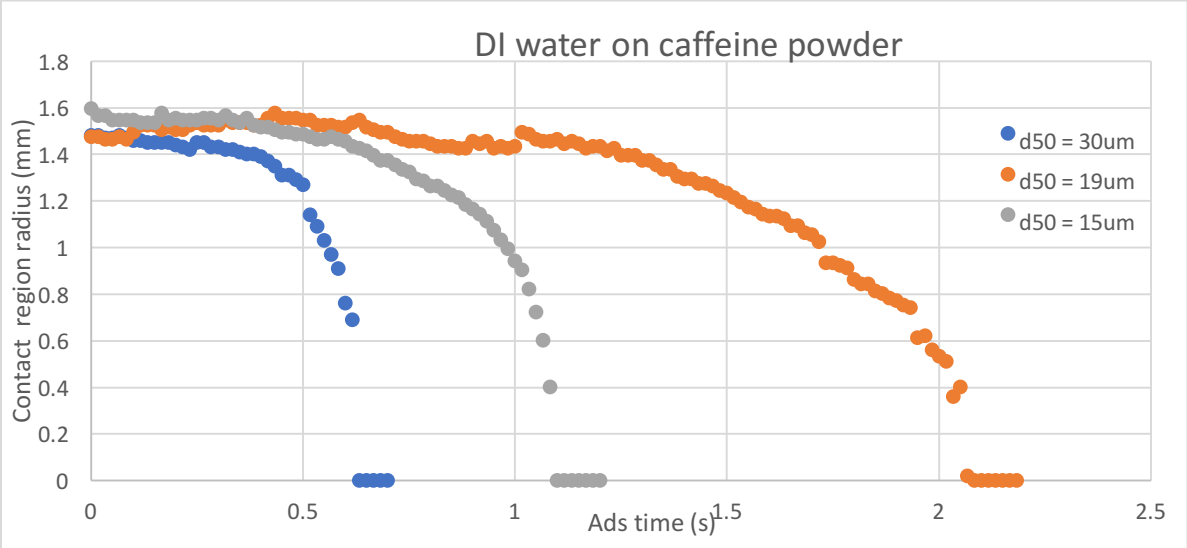
DI water on caffeine powder
Contact region radius (mm)
Ads time (s)
d50 = 30um
d50 = 19um
d50 = 15um
0
0.2
0.4
0.6
0.8
1
1.2
1.4
1.6
1.8
0.5
1
1.5
2
2.5

(c)

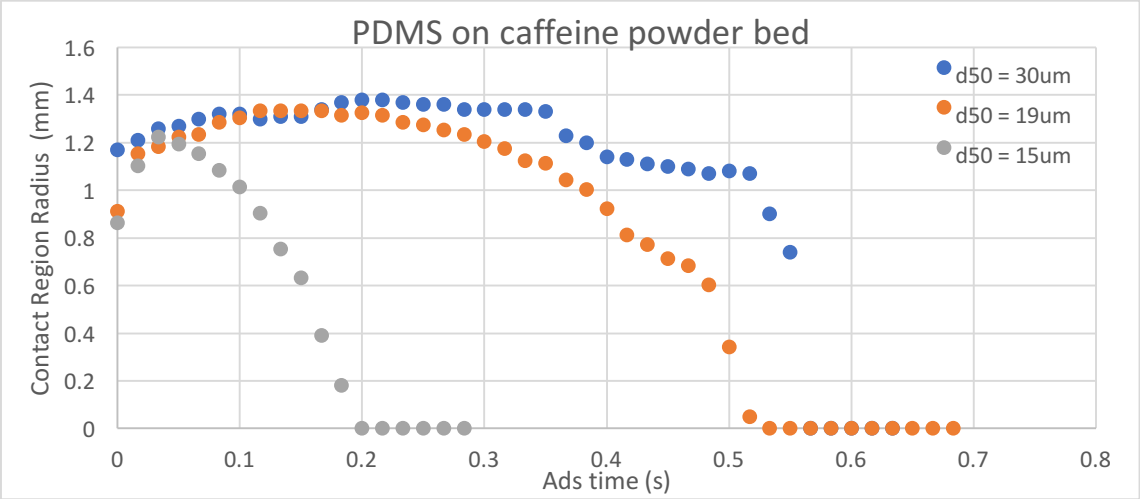

(d)

Fig 18 Penetration Profile of DI water and PDMS drop penetrating on the caffeine powder bed with different size distribution. (a), (b) Penetrated volume vs time for DI water and PDMS respectively; (c), (d) contact region radius vs time for DI water and PDMS respectively.

DI water and PDMS drops have quite similar initial volume respectively. From these profiles above, we can observe that the difference in particle size distribution does have a significant effect on the total penetration time of both DI water and PDMS drops. That's been said, we would expect smaller particle size with longer penetration time for DI water. However, behaviors of d50 = 15um caffeine powder are out of the trend we expected. Note that the average porosity of caffeine powder bed presented in the table above had a jump from 0.45 to 0.59 with the particle size distribution decreasing from d50 = 19um to d50 = 15um. The jump in porosity could be a factor to affect the penetration time.

The trend in penetration time for PDMS drops is reversed comparing to DI water, smaller the particle size smaller the penetration time.

Considering the contact radius, except the fast penetration of PDMS on caffeine powder d50 = 15um, the others showed a significant amount of constant radius time region. Note

that the maximum constant radius of drop is close with three different size distributions and similar initial volume for both liquids respectively.

A nondimensional time t' was defined as:

$$t' = t\frac{\gamma}{\mu {r_c}^2 \varepsilon} = \bar{t} \Big/ \frac{2k}{r_{eff}} cos\theta \tag{30}$$

In the case of powder beds made up of the same materials and the same applied pressure, the factor $\frac{2k}{\varepsilon r_{eff}}$ can be supposed as a constant. In addition, $\frac{2k}{\varepsilon r_{eff}} cos\theta$ is a constant if the liquid is the same. Then, for the same powder bed and liquid drop, if the profiles of dimensionless volume vs $(t' * \varepsilon)$ are overlapping, it means the profiles of dimensionless volume vs $\bar{t}$ should also be overlapping.

We present some examples of non-dimensional profile of caffeine powder d50 = 19um. In the figure below, the non-dimensional profiles from two different initial drop volume overlap with each other for both DI water and PDMS drop respectively. Run 1 and Run 2 have a smaller initial volume for DI water and PDMS drop respectively compared with Run 3,4 and 5. These indicate that there is little effect of initial drop volume on penetration dynamic and a universal function, which is independent of initial drop volume, between dimensionless volume and $\bar{t}$ could exist.

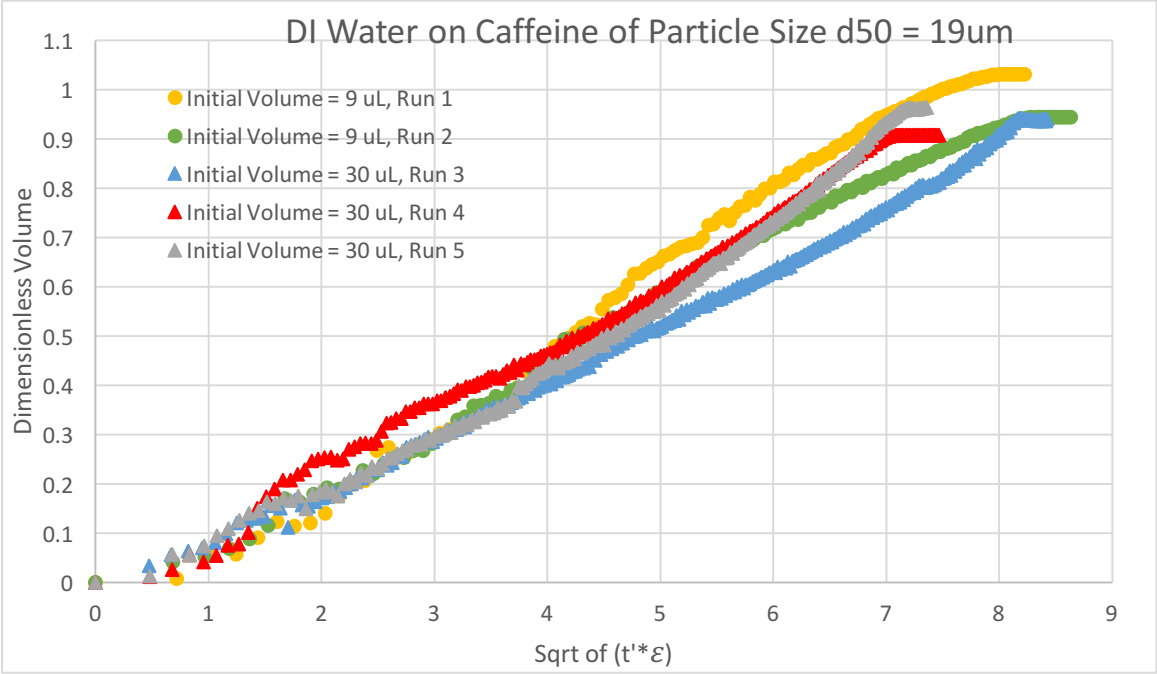

(a)

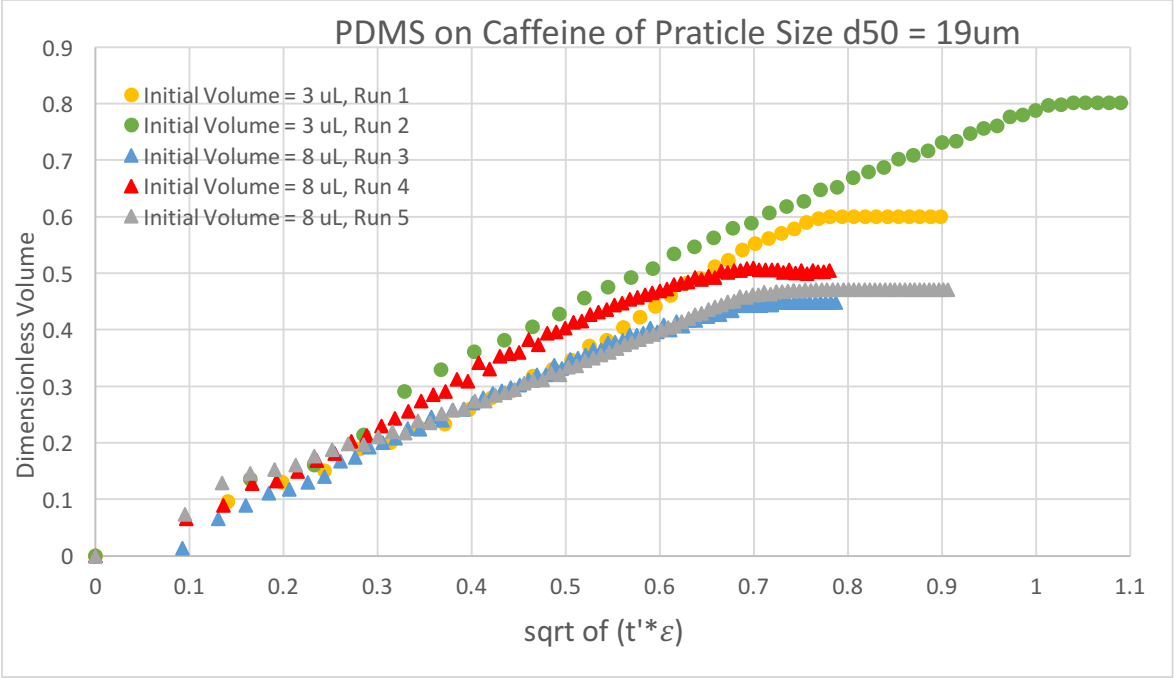

(b)

Fig 19. Non-dimensional volume vs sqrt of (t'*ε). (a) DI water drops with two initial volume, 9uL and 30uL; (b) PDMS drops with two initial volume 3uL and 8uL

Finally, we present some results of calculation of contact angle. In Fig 20 (a), we showed three single runs from three caffeine powder bed with different particle size distribution respectively. The contact angles seem to be consistent despite of the change of dimensionless volume. This consistence suggested the validation of our methods.

However, among different runs on the caffeine powder beds of same particle size distribution, the results are not as consistent as in the case of lactose powder bed. Especially for the case of d50 = 15um, the parallel experiments yield inconsistent results from earlier experiments 2 months ago. We suspected that during the storage properties including particle size of the smallest caffeine powder group might not be stable. For example, granular could form or decompose during the storage. That's been said, we only present the results of caffeine powder d50 = 15um in July, 2016 and those later close to it.

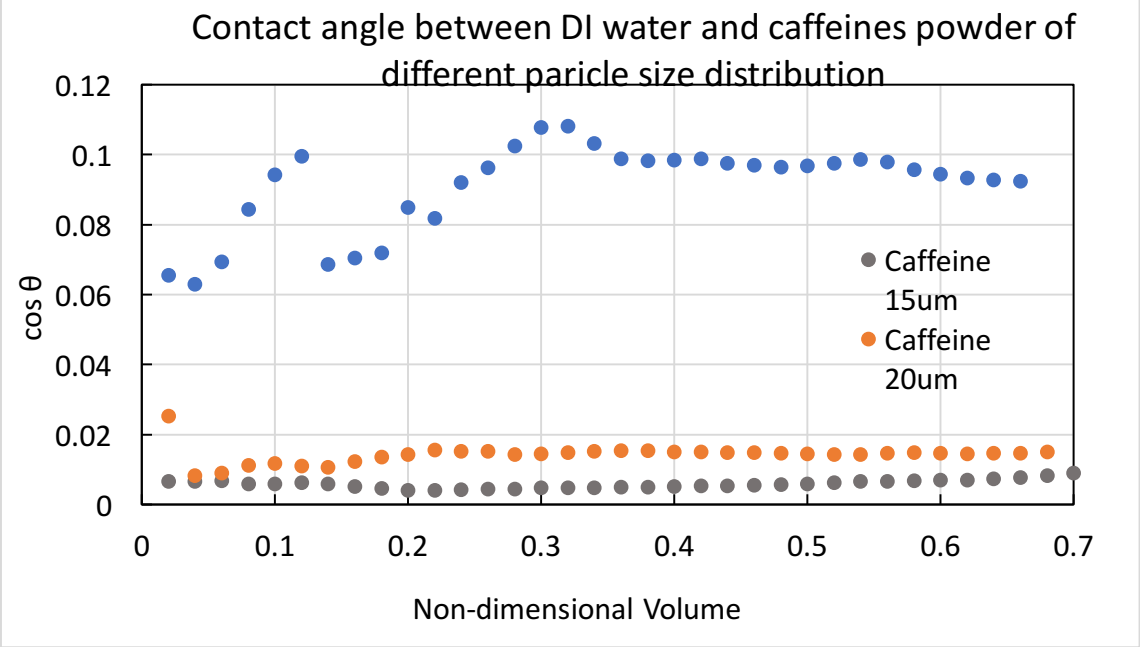

(a)

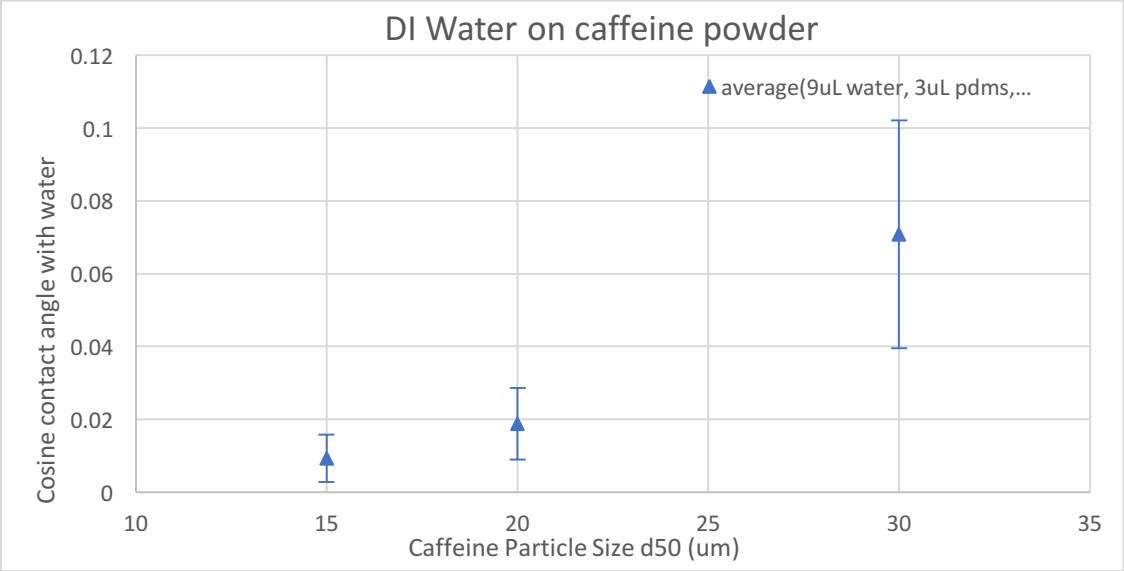

(b)

Fig 20. Cosine of contact angle between DI water and caffeine powder.

In Fig 20 (b), we present the average among different runs with error bar in the same condition that initial volume of water is 9uL and initial volume of PDMS drop is around 3uL. We collected the corresponding cosine value of dimensionless volume = 0.4 in each run and made average among them. The cosine of contact angle shifted to a lower number with smaller particle size distribution. The result suggested that caffeine powder of larger particle size distribution could yield smaller contact angle. And the results of d50 = 15um and 19um are close. It also suggested that there could be a minimum limitation cosine of contact angle near particle size of d50 = 15um.

Before getting to any solid conclusion, we still have some doubts concerning the caffeine powder case. For example, is there any effect of significant variation of powder bed porosity on the penetration dynamic? How could we explain and eliminate the inconsistence between different runs especially in the case of d50 = 15um? What could

be the effect of milling on contact angle measurement? Those questions need to be answered with investigations in the future.

Chapter 6. Summary & Conclusions

A droplet penetration method (DPM) was developed to characterize the wettability of pharmaceutical powders. Sessile droplets of two different liquids, used as *test* and *reference* liquids, were deposited on a slightly compressed powder bed and their penetration processes was recorded. Two simplifying assumptions are considered. First, the capillary pressure inside the porous powder is the only dominant driving force for the imbibition of drops. Second, the contact area between the penetrating drop and the powder bed is constant. Then, the penetration process in non-dimensional variables is independent of any dimensionless number. Hence, a *reference* liquid can be used to decouple the properties of the powder bed from the assessment of contact angle of the *test* liquid.

In this thesis, the effect of particle size distribution on the wetting behavior of pharmaceutical powders was investigated by the droplet penetration method. Two powder materials, an excipient and an active pharmaceutical ingredient (API), are used. The excipient is lactose monohydrate powder sieved to obtain particles in the following size ranges: 38-45, 45-53, 53-63, 63-75, 75-90, 90-106 μm. The API used is caffeine anhydrous powder with particle size distribution characterized by d50 = 15, 19 and 30 μm. Smaller caffeine powders are obtained by milling. In all cases, the test liquid is deionized water and the reference liquid used was silicone oil. It was found that lactose powders with a particle size smaller than 75 μm have approximately the same contact angle. However, there is a significant decrease in the calculated contact angle when particles are larger than 75 μm. In the case of caffeine, it was found that larger particles yield smaller contact angle.

In addition, we showed that non-dimensional penetration profiles of PDMS on lactose with various particle size, tend to collapse into one universal curve. It suggests wetting

behavior of PDMS is independent of particle size distribution of powder bed, and hence, PDMS could be a good reference liquid with low surface tension. We also showed the nondimensional penetration profiles on caffeine powder bed are independent of initial drop volume of DI water and PDMS respectively. Above all, observations of good overlapping among nondimensional profiles demonstrate the existence of a universal function between nondimensional wetted volume and nondimensioanl time.

Note that particle size distribution may affect the contact angle along with other factors, like particle shape, porosity etc. In the future work, we need to address these variables along with particle size distribution. For example, if the particle shape shifted with the variation of particle size, we will have to determine whether the effect on wetting behaviors resulting from particle size, particle shape or their combination.

Reference

Alghunaim, A. K. (2016). Techniques for determining contact angle and wettability of powders. *Powder Technology*, 287, 201-215.

Alleborn, N. &. (2004). Spreading and sorption of a droplet on a porous substrate. *Chemical Engineering Science*, 59(10), 2071-2088.

Bear, J. (2013). *Dynamics of fluids in porous media.* Courier Corporation.

Bosanquet, C. H. (1923). LV. On the flow of liquids into capillary tubes. *The London, Edinburgh, and Dublin Philosophical Magazine and Journal of Science*, 45(267), 525-531.

Buckton, G. (1993). Assessment of the wettability of pharmaceutical powders. *Journal of adhesion science and technology*, 7(3), 205-219.

Buczko, U. &. (2006). Assessing soil hydrophobicity and its variability through the soil profile using two different methods. *Soil Science Society of America Journal*, 70(3), 718-727.

Carman, P. C. (1956). *Flow of gases through porous media.* Academic press.

Dang-Vu, T. &. (2005). Characterization of porous materials by capillary rise method. . *Physicochemical problems of mineral processing*, 39, 47-65.

Daniel, R. C. (2006). Spreading on and penetration into thin, permeable print media: Application to ink-jet printing. *Advances in colloid and interface science*, 123, 439-469.

Denesuk, M. S. (1993). Capillary penetration of liquid droplets into porous materials. *Journal of colloid and interface science*, 158(1), 114-120.

Denesuk, M. Z. (1994). Dynamics of Incomplete Wetting on Porous Materials. *Journal of Colloid and interface science*, 168(1), 142-151.

Depalo, A. &. (2013). Wetting dynamics and contact angles of powders studied through capillary rise experiments. *Colloids and Surfaces A: Physicochemical and Engineering Aspects*, 436, 371-379.

Dullien, F. A. (2012). *Porous media: fluid transport and pore structure. .* Academic press.

Gambaryan-Roisman, T. (2014). Liquids on porous layers: wetting, imbibition and transport processes. *Current Opinion in Colloid & Interface Science*, 19(4), 320-335.

Guo, J.-H. (2004, June). Lactose in Pharmaceutical Applications. *Drug Development & Delivery, 4*(5).

Hapgood, K. P. (2002). Drop penetration into porous powder beds. *Journal of Colloid and Interface Science*, 253(2), 353-366.

Hapgood, K. P. (2003). Nucleation regime map for liquid bound granules. *AIChE Journal*, 49(2), 350-361.

Holm, R. B. (2016). Investigation of surface porosity measurements and compaction pressure as means to ensure consistent contact angle determinations. . *International journal of pharmaceutics*, 498(1), 355-361.

Kirchberg, S. A. (2011). Influence of particle shape and size on the wetting behavior of soft magnetic micropowders. *Powder Technology*, 207(1), 311-317.

Kossen, N. W. (1965). The determination of the contact angle for systems with a powder. *Chemical Engineering Science*, 20(6), 593-599.

Lerk, C. F. (1976). Contact angles and wetting of pharmaceutical powders. *Journal of pharmaceutical sciences*, 65(6), 843-847.

Liu, Z. W. (2017). Capillary drop penetration method to characterize the liquid wetting of powders. *Langmuir*, 33(1), 56.

Navaz, H. K. (2008). Sessile droplet spread into porous substrates—Determination of capillary pressure using a continuum approach. *Journal of colloid and interface science*, 325(2), 440-446.

Nehlig, A. D. (1992). Caffeine and the central nervous system: mechanisms of action, biochemical, metabolic and psychostimulant effects. *Brain Research Reviews*, 17(2), 139-170.

Nguyen, T. H. (2010). Effect of formulation hydrophobicity on drug distribution in wet granulation. . *Chemical Engineering Journal*, 164(2), 330-339.

Pawar, P. J. (2016). The effect of mechanical strain on properties of lubricated tablets compacted at different pressures. *Powder Technology*, 301, 657-664.

Pepin, X. B. (1999). Powder dynamic contact angle data in the pharmaceutical industry. . *Pharmaceutical science & technology today*, 2(3), 111-118.

Quéré, D. (1997). Inertial capillarity. *EPL (Europhysics Letters)*, 39(5), 533.

Razavi, S. M. (2016). Toward predicting tensile strength of pharmaceutical tablets by ultrasound measurement in continuous manufacturing. *International journal of pharmaceutics*, 507(1), 83-89.

Ridgway, C. J. (2002). Effect of capillary element aspect ratio on the dynamic imbibition within porous networks. . *Journal of Colloid and Interface Science*, 252(2), 373-382.

Stevens, N. R. (2009). The uniform capillary model for packed beds and particle wettability. *Journal of colloid and interface science*, 337(1), 162-169.

Xiao, J. S. (2012). Source-like Solution for Radial Imbibition into a Homogeneous Semi-Infinite Porous Medium. *Langmuir*, 28(9), 4208-4212.

Zhang, D. F. (2002). Wettability of pharmaceutical solids: its measurement and influence on wet granulation. *Colloids and Surfaces A: Physicochemical and Engineering Aspects*, 206(1), 547-554.